The properties of the Miocene coal seams in the Soma Basin (W. Turkey): Insights from coal petrography, Rock-Eval pyrolysis, mineralogy and elemental contents

Ali İhsan Karayiğit[a*], Ralf Littke[b], Xavier Querol[c], Tim Jones[d], R. Görkem Oskay[a**], Kimon Christanis[e]

[a] Hacettepe University, Department of Geological Engineering, 06800, Ankara/Turkey
[b] Institute of Geology and Geochemistry of Petroleum and Coal, Energy and Mineral Resources (EMR), RWTH Aachen University, Lochnerstr. 4-20, 52056 Aachen, Germany
[c] Institute of Environmental Assessment and Water Research (IDÆA), Consejo Superior de Investigaciones Científicas (CSIC), C/ JordiGirona 18-26, 08034 Barcelona, Spain
[d] Department of Earth Sciences, Cardiff University, Cardiff CF1 3YE, Wales, UK
[e] University of Patras, Department of Geology, Rio-Patras, Greece

Abstract

The Soma Basin hosts three coal seams (kM2, kM3 and kP1) and several altered tuff layers within the Miocene sequences. This study focuses on the determination of coal petrography, Rock-Eval pyrolysis, mineralogy and elemental contents of the three coal seams from Eynez, Işıklar and Deniş sectors in the basin, and to identify the mineralogy of altered tuff layers within kM2 and kP1 seams. The routine coal quality analyses show that coal samples from the kM2 seam are characterized by lower ash yields and total S contents, and higher gross calorific values than kM3 and kP1 seams. The mineralogical composition of the bulk coal samples from the kM2 seam is made up mainly of quartz, clay minerals and lesser amounts of feldspars and carbonates. In the kM3 and as well as in the lower part of kP1 seam carbonate minerals are ~~being~~ dominant phases due to the existences of fossil shell-bearing bands in the coal beds and intercalations. The statistical data implies that major elements in bulk coal samples, such as Al, Fe, K, Mg and Na, and the vast majority of minor and trace elements, as we expected, have inorganic affinity. The trace element contents and elemental enrichments are generally changeable from seam to seam; nevertheless, Cs, Li and U are commonly enriched in all studied coal seams. These could be related to the differences i~~o~~n ash yields and mineralogical compositions of coal beds within the seams. The mineralogical compositions of the altered tuff layers identified within the kM2 and kP1 seams display similar compositions with tonsteins; therefore, these layers are presumably in air-fall ash that were originated from synchronous felsic volcanic activities around the basin. The existence~~s~~ of volcanic layers also ~~have~~ has some influence~~s~~ on the mineralogical and elemental composition of both seams. The SEM data shows that clay minerals originated from these layers and certain trace elements (e.g. As and Zr) are

enriched in the coal layers below the tuff layers in the kM2 seam. This might be related to penetration of leached pore waters into these layers and precipitation of epigenetic minerals.

The coal petrography data and coal facies diagram show that precursor peat of the kM2 seam was accumulating under telmatic, mesotrophic anoxic conditions where the water level was high and stable. The relatively low ash yields and thicker coal beds suggest ~~the~~ a lower clastic input ratio from the margins; therefore, the aluminosilicate affiliated elements display lower concentrations in this seam. Following periods when the~~,~~ water-table fluctuated several times and covered entire mire surface~~; thus~~, peat formation ceased and several clastic and calcareous intercalations were deposited in the kM3 and kP1 seams. These imply the development of limno-telmatic conditions where fluvial influences took places during peat accumulation of both seams. Therefore, clastic inputs from the margins were high which resulted in elevated ~~the~~ concentrations of aluminosilicate affiliated elements. Furthermore, the mineralogical compositions of coal and intercalations of both seams also suggest the development of neutral to alkaline conditions. Considering the maceral compositions along with the thickness of coal, coal seams in the Soma Basin might have and can ~~suggest the~~indicate oil generation potential; however, the ~~data of~~ pyrolysis analysis data shows that the studied coal seams are mainly gas-prone and only certain coal beds have mixed hydrocarbon generation capacity. Nevertheless, the changes of~~n~~ vegetation and depositional conditions also ~~have~~ reflect~~ions~~ on the HI values. The slightly higher HI and TOC in the kM2 seems to be related to high contribution of woody material in peat and the development of more acidic conditions, whereas the predominance of herbaceous plant and alkaline conditions in the kM3 and kP1seams resulted in relative low HI and TOC values. All data presented in this study indicates that lithological features, differences in coal qualities and elemental contents in the Soma Basin were mainly controlled by changes i~~o~~n the depositional conditions and as well as detrital inputs during Miocene.

Keywords: Coal, element, Rock-Eval pyrolysis, coal facies, air-fall ash, Miocene, Soma, Turkey

* Corresponding author, **visiting scholar

1. Introduction

The regional extensional tectonic regime during late Cenozoic resulted in the development of regional volcanic activity and the formation of several NW–SE and NE–SW trending grabens in ~~the~~ western Turkey (Seyitoğlu and Scott, 1991; Yılmaz et al., 2000). The terrestrial conditions ~~were~~ also predominant during the Neogene and all these grabens filled with alluvial, fluvial and lacustrine deposits, and as well as volcano-sedimentary rocks. The suitable climatic conditions along with constant subsidence also allowed peat accumulation within these basins during Miocene; therefore, several economic coal deposits are located within Miocene lacustrine and terrestrial sequences in ~~the~~ western Turkey (Toprak, 2009; Kayseri-Özer, 2016).

The Soma Basin is relatively smaller than other basins in western Turkey; however, it hosts the most significant coal deposit due to its geological setting and coal reserves. The total coal reserve of the Soma ~~basin~~ Basin is about 738 Mt, and 10.4 Mt of coal~~s~~ are ~~producing~~ produced annually by mainly open-pit mines, of which 7.7 Mt are ~~consuming~~ consumed in Soma coal-fired power plants with 990 MW capacity and 2.7 Mt are ~~using~~ used in domestic and industrial purposes (TKİ-ELİ, 2015). The basin is divided into several sectors, and hosts three coal seams, namely kM2 (lower-seam), kM3 (middle-seam) and kP1 (upper-seam). The coal characteristics and thickness of these seams are changeable from sector to sector (Tuncalı et al., 2002). Another distinct feature of the Soma Basin is the presence of several altered tuff layers and basaltic intrusions within the coal seams (Karayiğit and Whateley, 1997). The ash layers, particularly identified in the kM2 seam, could be useful for stratigraphic correlation during underground mining operations and can also give information about mineral inputs during peat accumulation.

There are several studies from the Soma Basin that mainly focused on geological setting, palaeopalynological, as well as environmental and economic aspects (Nebert, 1978; Akgün et al., 1986; Gemici et al., 1991; Takahashi and Jux, 1991; Akgün, 1993; İnci, 1998a, b, 2002; Karayiğit et al., 2000, 2006; Vassilev et al., 2005; Tercan et al., 2013; Hokerek and Ozcelik, 2015; Baysal et al., 2016; Kayseri-Özer, 2016). Coal-petrographical and geochemical studies are limited (Karayiğit and Whateley, 1997; Karayiğit, 1998; Tuncalı et al., 2002; Bulut and Karayiğit, 2006; Toprak, 2009). A~~Nevertheless, a~~ll these studies focused on either certain mining sectors or feed~~ing~~ coals to coal-fired power plants, and none of them reported any correlations between coal seams within the basin. ~~Noteworthy~~It is noteworthy that, any detailed study on altered tuff layers within the coal seams are also absent. In this paper, the main goal is to determine coal characteristics, reconstruct the palaeoenvironmental conditions during peat

accumulation, and oil-and gas-generation potential of the kM2, kM3 and kP1 coal seams in the Eynez, Işıklar and Deniş sectors, using coal petrography, Rock-Eval pyrolysis, mineralogy and geochemical techniques. The specific objection of the study is to ~~find out~~identify the features of tuff layers within the seams and ~~its~~ their impacts on mineralogical and elemental compositions of the coal seams.

2. Geological setting

The Soma Basin is a NE–SW trending, approximately 20-km long and 5-km wide, fault controlled basin in western Turkey (Seyitoğlu and Scott, 1991; İnci, 2002). The margins of the basin are mainly built of Upper Cretaceous-Palaeocene carbonates (recrystallized limestone) and Miocene volcanic rocks; furthermore, greywacke and diabase blocks ~~are~~ outcropped ~~out~~ in a small area on southern margin (Fig. 1). The regional extensional tectonics initiated during the early Miocene ~~and~~ created depositional space for the basinal infillings (Nebert, 1978; Seyitoğlu and Scott, 1996; İnci, 1998a); consequently, the major coal-bearing Soma Formation ~~commenced to~~started deposition during ~~Early~~ early to ~~Middle~~ middle Miocene (Benda, 1971; İnci, 2002). The F~~f~~ormation is composed~~s~~ of alluvial sediments and lacustrine carbonates (Fig. 1). The kM2 and kM3 seams are located in this F~~f~~ormation (Fig. 1b). The total thickness of the kM2 seam can reach up to 27 m, whereas the kM3 seam with thicker calcareous intercalations can reach up to 15 m. The Deniş Formation, which overlies the Soma Formation, ~~commenced to~~started with alluvial sediments and turned to fluvial sediments and lacustrine carbonates where the kP1 seam is located (İnci, 2002). The total thickness of the kP1 seam is changeable within the basin, and it is only mineable in the Deniş sector. This seam hosts several coal beds and thick intercalations; therefore, it can be divided into lower, middle and upper parts. The Pliocene Soma volcanics overlie the Deniş Formation (Fig. 1). Furthermore, basaltic intrusions were also ~~invaded~~ implaced in the Soma Basin during the Pliocene-Pleistocene and these caused ~~to~~ the development of contact metamorphism in the kM2 coal seam. Thus, natural coke occurrences were identified near to the contact zone (Karayiğit and Whateley, 1997; Karayiğit, 1998). Finally, Quaternary unconsolidated sediments ~~are~~ unconformably overlie the older units (Fig. 1b).

3. Material and methods

A total of 64 coal samples and 16 intercalations, of which 6 samples are from altered tuff layers, were gathered using channel sampling technique from five profiles in the Eynez, Işıklar

and Deniş sectors (Fig. 2). The kM2 seam was sampled from Eynez, Işıklar and Deniş sectors, whereas kM3 was only sampled in the Işıklar sector and kP1 in the Deniş sector.

Standard proximate and ultimate analyses were conducted according to ASTM standards (ASTM D3175, 2011; ASTM D3174, 2012; ASTM D3302, 2015; ASTM D5373, 2016). The gross calorific values were determined in an IKA 4000 adiabatic calorimeter (ASTM D5865, 2013) at Hacettepe University. The petrographic analysis was performed from polished coal blocks, prepared according to ISO 7404–2 (2009) standard, and these blocks were examined in oil immersion under both white incident light and blue-light excitation using a Zeiss Axioplan coal-petrography microscope at RWTH Aachen University and a Leica DM4000M microscope at Hacettepe University. The identification of macerals followed the Stopes-Heerlen nomenclature, modified after the ICCP System 1994 (International Committee for Coal and Organic Petrology, ICCP, 2001; Sýkorová et al., 2005; Pickel et al., 2017). Random huminite reflectance was measured on ulminite according to International Standard Organization (ISO) 7404-5 (2009). The mineralogical composition of bulk coal and inorganic samples were determined using an X-ray diffractometer with a Cu anode tube at Hacettepe University and Cardiff University. The clay fraction analysis (XRD-CF) was also carried out from selected inorganic samples at Hacettepe University.

The Rock-Eval pyrolysis analysis was conducted in order to determine the T_{max}, hydrogen index (HI) and the oxygen index (OI) values according to procedure described by Espitalié et al. (1977a, b). Total organic carbon (TOC) and inorganic carbon (TIC) contents were measured using a LECO RC-412 Multiphase C/H/H_2O Analyzer at RWTH Aachen University. Combustion took place using oxygen gas at temperatures between 350 °C and 520 °C for TOC and 520 °C and 1050 °C for TIC. Moreover, a brief organic geochemistry analysis performed on two bulk coal samples one from the kM2 seam (E-9) and another from the kP1 seam (D-6) using Soxhlet-extraction with dichloromethane and GC-MS.

The elemental composition was determined by means of Inductively Coupled Plasma Atomic Emission Spectrometry (ICP-AES) and Inductively Coupled Plasma Mass Spectrometry (ICP-MS) at the Institute of Environmental Assessment and Water Research (IDAEA) applying the technique described in detail by Querol et al. (1995). Selected polished blocks of coal and tuff samples were carbon coated and examined under SEM equipment ~~settled~~ situated at Hacettepe University, Cardiff University and RWTH Aachen University in order to

have better understanding mineralogical composition and as well as trace elements hosted in the minerals.

4. Results

4.1. Macroscopic features and proximate analysis

The matrix-lithotype is commonly identified from the kM2 seam and mineral-rich lithotypes are more abundant in the kM3 seam and particularly the middle and upper parts of the kP1 seam. The gastropod fossil shell-bearing coal beds were identified more frequently in the kM3 seam and lower parts of the kP1 seam, whereas the clay bands within coal beds were abundant in the upper section of the kP1 seam (Fig. 2). The floor rocks mainly compose of claystone and the roof rocks are clayey limestone/marl. The kM2 seam hosts thin intercalations and mainly compose of claystone/clayey limestone (Fig. 2). The kM3 seam hosts mainly calcareous intercalations, whereas gastropod-bearing claystones are more abundant in the kP1 seam. Furthermore, altered tuff layers were mainly identified from kM2 seam at Eynez and Işıklar sectors (Fig. 2) and also one layer was identified from kP1 seam at the Deniş sector.

The results of proximate analysis along with gross calorific values indicate that there are several significant differences between the coal seams in the Soma Basin (Table 1). The ash yields in the kM2 seam are generally lower than other seams. The ash yields with more than 50% are mostly related to frequent existence of gastropod remains within coal beds in kM3 and kP1 seams. In turn, high volatile matter contents (up to 67.6%, on dry, ash-free basis) and low calorific values are recorded (Table 1). The proximate analysis results and calorific values are generally in agreement with the previous studies; beside, higher ash yields are only reported from kP1 in this study (Karayiğit et al., 2000; Tuncalı et al., 2002; Tercan et al., 2013). This may be related to differences of sampling intervals and/or location of sampling profile in the Deniş sector.

4.2. Maceral composition and rank

All three maceral groups (huminite, liptinite and inertinite) are determined with various proportions from the three coal seams (Table 2). Huminite is the dominant maceral group (up to 84.9 vol.% on whole coal basis) and its proportions are slightly increased towards upper parts of the kM2 and kM3 seams and decreased in the kP1 seam. The kM2 seam is characterized by

high telohuminite proportions and the highest value was recorded at the Deniş sector (61.2 vol.%), whereas the kM3 and kP1 seams contain higher proportions of detrohuminite (Table 2). Ulminite, mainly eu-ulminite, is ~~the~~ predominant within the telohuminite subgroup; however, texto-ulminite is ~~being~~ predominant in samples of the kM2 seam from Işıklar and Deniş sectors. Furthermore, ulminite macerals are well gelified in Eynez and Işıklar (both kM2 and kM3 seams) sectors. Textinite contents are low (≤1 vol.%) in the samples. The cell-lumens of textinites are generally filled with corpohuminite, resinite and/or mineral matter (Fig. 3). Densinite is ~~the~~ predominant within the detrohuminite group and inertodetrinites, liptodetrinites and sporinites were mostly associated with densinite (Fig. 3). Gelohuminite is also commonly observed in all studied samples (Table 2). Corpohuminite is the dominant maceral in this subgroup (up to 11.5 vol.%). Gelinite, however, is ~~being~~ more commonly the gelohuminite maceral in lower and middle parts of the kP1 seam. Liptinite was also commonly observed in all samples (1.7 and 16.9 vol.%) and liptodetrinite is the predominant liptinite maceral. In addition, liptinite contents are slightly high in the kM2 seam where resinites were also commonly identified. Inertinite contents are generally low in the kM2 seam (≤1 vol.%), whereas these are slightly higher than others (up to 11.0 vol.%) in the kM3 seam and increased upwards ~~of~~ in the seam. Minerals identified under coal-petrography microscopy are mainly clay minerals, carbonates (calcite and siderite) and pyrite. The gastropod shell fragments are commonly observed during coal-petrography studies. The maceral compositions of the studied samples are generally in agreement with the previous coal petrography studies from the Soma Basin (Karayiğit and Whateley, 1997; Karayiğit, 1998; Tuncalı et al., 2002; Bulut and Karayiğit, 2006; Karayiğit et al., 2010, 2012; Toprak, 2009).

The random huminite reflectance (%R_o) values in ulminite (especially eu-ulminite B) vary between 0.36 and 0.46%. The higher %R_o values measured from the kM2 seam at the Eynez sector and the kM3 seam at the Işıklar sector, and low R_o values measured from the kM2 seam at the Deniş sector (Table 2). Considering the presence of basalt dykes i~~o~~n the adjacent areas of Eynez and Işıklar sectors (Karayiğit, 1998), deeper burial depths and presence of well-gelified ulminites in these sectors, the low R_o values from the kM2 seam in the Deniş sector can be expected. The reflectance data is in agreement with previous studies (Karayiğit and Whateley, 1997; Tuncalı et al., 2002; Toprak, 2009). The mean random reflectance values along with calorific values and ash yields of the kM2 and kM3 indicate coal samples are medium- to high-grade, low rank A to medium rank D coal and subbituminous (low-rank A) according to ECE-UN (1998) and ISO 11760 (2005) classifications, respectively. Coal samples from the kP1

seam are low- to medium-grade low rank C to B coal and lignite (low-rank B) to subbituminous (low-rank A).

4.3. Bulk geochemical parameters

The kM2 seam is characterized by high total carbon (34.5-64.5%; on dry basis) and low total sulphur (0.2-2.1%; on dry basis) contents, while in the kM3 and kP1 seams coal samples display higher total S and lower total C content (Table 1). The Rock Eval analysis data of all the samples reveals that S1, S2 and S3 values are ranging from 0.6 to 3.7 mg HC/g, 22.2 to 107.2 mg HC/g, 3.2 to 19.4 mg HC/g coal, respectively. The mean S1 and S2 values are higher in the kM2 seam (Table 1). Total organic carbon (TOC) values of the kM2 seam range from 32.5 to 64.4 wt.% (on air-dried basis) and their mean values are relatively higher than other seams. In kM3 and kP1 seams TOC values vary from 23.4 to 54.8 wt.% (avg. 38.0 wt%) and 17.9 to 56.9 wt.% (avg. 31.1 wt%). As expected, total inorganic carbon (TIC) contents are relatively high in fossil shell-bearing samples (Table 1). Moreover, TOC values increase throughout upper parts of the kM2 and kM3 seams where ash yields decrease. The total sulphur contents of the seams in the Soma Formation display a slight increase upwards; in addition to this, higher total sulphur contents are generally recorded over and below ~~of~~ altered tuff layers in the kM2 seam. In contrast, while ash yields increase upwards of the kP1 seam, TOC values, total carbon and sulphur contents decrease.

The measured Hydrogen Index (HI) values of studied samples are generally low and range from 76 to 178 mg HC/g TOC (Fig. 4 and Table 1), and their calculated HI_{max} values on the HI-VR diagram are between 241 and 278 mg HC/g TOC (Fig. 5). The oxygen index (OI) is generally low (≤41 mg CO_2/ g TOC; Fig. 4a and Table 1). T_{max} values vary between 392 and 439 °C and are characteristic for a low-rank coal. The HI *vs*. OI and HI *vs.* T_{max} diagrams (Fig. 4) show that kerogen type III is dominant in all seams and in some samples mixed type III-IV are ~~being~~ common (Tissot and Welte, 1984). Furthermore, plotting data on HI *vs.* T_{max} diagram indicates that the coal samples from kM2 and kM3 are immature to early mature and samples from the kP1 seam are clearly immature (Esphlie et al. 1977a, b, 1984). Overall, the results of Rock-Eval analysis indicate the coal samples have a heterogeneity in organic matter type and in such cases are characteristic for low-rank coals (Petersen et al., 2009; Escobar et al., 2016). This heterogeneity is also in agreement with coal petrography data. For instance, changes i~~o~~n HI values seem to be related to variable maceral contents in the coal samples (Hunt, 1991;

Petersen and Rosenberg, 2000; Kalaitzidis et al., 2009; Petersen et al., 2009; Gross et al., 2015). The kM2 seam display higher telohuminite and HI values, whereas relatively low HI and high OI and S3 values can be testimony for relatively high ~~in~~ inertinite contents of the kM3 seam. The high total sulphur contents generally tend to elevate HI values (Petersen, 2006); in contrast, the effect of total sulphur on HI values in the studied samples might be limited due to their low maturity.

4.4 Molecular organic geochemistry

The results of molecular organic geochemistry analysis ~~could~~ give a basic ~~knowledge~~ understanding about the predominant peat-forming vegetation in the kM2 and kP1 seams. Most abundant substances in the aliphatic fraction of the analysed coal samples can be attributed to cyclic sesquiterpenes and cyclic diterpenes. The sample E-9 (kM2 seam) was extremely dominated by these substances (Fig. 6a). Beside cyclic sesquiterpenes and cyclic diterpenes, *n*-alkenes were also present with their chain lengths between 10 and 31 carbon atoms. In both samples (E-9 and D-6) a bimodal distribution with maxima at C_{14}/C_{15} and around C_{23}/C_{25} were observed. Sample D-6 (kP1 seam) exhibits the highest concentrations of *n*-alkenes at $C_{23}/C_{25}/C_{27}/C_{29}$ (Fig.6b), but the *n*-alkenes of sample E-9 maximised at C_{14}/C_{15} (Fig. 6a). The maxima in the range of C_{23} and C_{25} (Fig. 6b) are characteristic~~s~~ for a high contribution of freshwater aquatic macrophytes (Ficken et al., 2000), whereas *n*-alkenes with chain lengths of more than 29 carbon atoms can be attributed to the input of organic matter derived from higher land plants (Volkman, 1986; Canuel et al., 1997). These distributions are in agreement with coal petrography data. The telohuminite group is predominant in the sample E-9 and the sample D-6 display higher detrohuminite contents. Furthermore, the *n*-alkene distributions of both samples are characterized significantly by an odd-over-even predominance indicating they are immature.

4.5. Mineralogy

4.5.1. Minerals in intercalations and altered tuff layers

The common carbonate minerals in the intercalations are calcite, dolomite and siderite, and they are the dominant phases in the clayey limestone/marl (Table 3). Moreover, aragonite is only identified in gastropod fossil shell-bearing samples. The clay minerals are the dominant phase in claystones and minor phases in the calcareous intercalations (Table 3). The results of XRD-CF analyses indicate that kaolinite and smectite are common in clay-fraction minerals in

the kM2 seam, whereas in the kP1 seam illite is ~~being~~ more common together with kaolinite. Quartz and feldspar are abundant to minor phases in the claystones; nevertheless, quartz is the dominant phase in the fined~~-~~-grained sandstone in the kM2 seam. Opal/CT is traced only from claystones in kM2 and kP1 seams where altered tuff layers are identified. Pyrite is also traced from in a few samples from kM2 and kP1 seams (Table 3). The predominance of silicate minerals in the intercalations imply that these are presumably brought by fluvial inputs from marginal areas (e.g. volcanic rocks). In contrast, the Ca-rich water ~~support~~s that originated from karstic aquifers and lacustrine conditions allowed the formation of carbonate minerals, particularly in the kM3 seam and lower parts of the kP1 seam. Similar suggestions were also reported from the previous study in the basin (İnci, 1998a).

The mineralogical compositions of tuff layers in the kM2 and kP1 seams are slightly different than other intercalations. The clay minerals are the dominant phase in all layers according to XRD results, and the abundant phases are quartz and feldspars (Table 4). Furthermore, carbonate minerals (calcite and dolomite) and opal/CT are traced in some altered tuff samples. The SEM-EDX data shows a variety of accessory minerals in these layers (Table 4 and, Figs. 7 and 8). The accessory minerals are biotites with Ti traces, phosphates (Cl-apatite and crandallite), zircon, Ti-oxides, ilmenite, titanite, REE-bearing silicates (e.g. allanite), and sulphides (pyrite, sphalerite and chalcopyrite). Beside sulphide and carbonate minerals, all these accessory minerals are identified as typical minerals for tonsteins (Bohor and Triplehorn, 1993; Ruppert and Moore, 1993; Dai et al., 2011; Spears, 2012). The minerals such as quartz, biotite, feldspars, opal/CT, Cl-apatite and zircon are primary products of volcanic inputs. Zircon and Cl-apatite are dominantly euhedral crystals (Fig. 7) that are characteristic for volcanic origin and also such crystals can be indicators for short distance transportation (Burger et al., 2002; Spears, 2012; Arbuzov et al., 2016). Feldspar in the altered tuff layers could also provide ~~knowledge~~ indications about the volcanic activity around the basin during the Miocene. The SEM-EDX data shows plagioclase is more commonly determined in the analysed tuff samples from kM2 seam, and alkali feldspars are predominant feldspar mineral in the sample from kP1 seam. This difference is presumably related to changes on chemistry of volcanic rocks during the Miocene around the Soma Basin (Ersoy et al., 2012).

The kaolinite is observed in the altered tuff layers as individual bodies (vermicules?), which are associated with biotites, or around feldspar or compose~~d~~d of the matrix of mineral aggregates (Figs. 7 and 8). The latter one contains traces of mostly Ti, and lesser Fe and K and the existence of these trace~~d~~ elements revealed that kaolinite~~s~~ are mainly alteration by-products of biotite ~~and~~

as well as feldspars. Such alterations are expected considering the freshwater environments in the Soma Basin. The presences of pyrite blades (Fig. 7) and the absence of zeolite minerals also imply the alteration of tuff layers took place in the open system under slightly acidic conditions (Querol et al., 1997; Bechtel et al., 2014). Nevertheless, the rare presence of carbonates indicating neutral conditions was also occurred. Other sulphide minerals like sphalerite and chalcopyrite seem to be developed from leached waters during diagenetic stages (Arbuzov et al., 2016). The acidic condition might also allow the reaction between weathered glass and P derived from organic matter (Triplehorn, 1990), thus, the identified alumina-phosphates in the samples might be formed in such way. Furthermore, allanite can be easily altered in the depositional environment (Bohor and Triplehorn, 1993); however, its presence in the ash layer in the kP1 seam suggests that the alteration of the tuff layers was presumably not dense as ~~like as~~seen in the kM2 seam. Overall, the mineralogical composition of altered tuff layers denoted that these are supposed to be originating from intermediate and/or felsic volcanic rocks. Therefore, these tuff layers in kM2 and kP1 seams were derived from synchronous volcanic activities developed around the basin.

4.5.2. Minerals in coal samples

The dominant phases present in the kM2 seam are quartz and clay minerals based on XRD data, whereas calcite is also ~~being~~ dominant in certain coal samples from Işıklar and Deniş sectors (Table 5). Other carbonate minerals identified from the kM2 seam are dolomite and siderite. Nevertheless, carbonate minerals are ~~being~~ the dominant phase in the kM3, where fossil shell remains are commonly observed, and here aragonite is also identified. The upper part of the kP1 seam is characterized by the predominance of clay minerals, while calcite along with quartz is being more common i~~o~~n the lower part. Feldspars and pyrite are generally minor phase in the three seams (Table 5). Additionally, opal/CT, and gypsum are also traced in few samples.

The SEM data is in agreement with the XRD data and provide a variety of accessory minerals (Figs. 9-12), such as ankerite, apatite, barite, biotite, chalcopyrite, chromite, monazite, sphalerite, titanite, Ti-oxides and zircon. Furthermore, calcareous fossil shell-fragments are commonly observed (Figs. 10 and 12) and fossil bone remains ~~in~~ of Ca-phosphate composition were also identified in few samples (Fig. 9).

The dominance of silicate minerals in bulk coal samples from the kM2 seam and the upper part of the kP1 seam could indicate continuous detrital input into palaeomire that suppressed

authigenic mineral formation. The SEM data shows the existence of individual kaolinite (vermicules?) and the clay aggregates with other minerals (e.g. feldspar, quartz, biotite, apatite, Ti-oxides and zircon) and organic matter (Figs. 9 and 10). Such aggregates are generally related to clastic inputs from margins. Besides, low ash yields from the kM2 seam along with thin intercalations imply the clastic input ratios ~~supposed to be~~were low during peat accumulation. Thus, clay minerals in the kM2 seam seem to be derived from another source rather than marginal clastic input. The matrixes of clay mineral aggregates are mostly Ti- and Fe-bearing kaolinites according to the SEM-EDX data (Fig. 9). Furthermore, feldspar and biotite crystals are altered within these aggregates as like the tuff samples. The individual kaolinites and their textures in the coal samples are also typical for kaolinites in tonsteins (Bohor and Triplehorn, 1993; Burger et al., 2000; Perama et al., 2013). Therefore, kaolinite and as well as clay aggregates are clastic inputs mainly derived from altered tuff layers and volcanic rocks on the margins and a lesser extent of alteration of feldspar and biotites in the palaeomire.

~~Similar~~ As seen with the tuff layers, the common varieties of feldspars are changeable seam to seam. SEM studies indicate that plagioclase is more commonly identified on the kM2, whereas alkali feldspars are more common in the kM3 and kP1 seams. This is, as explained previously, related to changes on chemistry of volcanic products during the Miocene (Ersoy et al., 2012). Furthermore, apatite, Ti-oxides and zircon were also observed within feldspar crystals and these inclusions are other indicators for clastic inputs from volcanic rocks on the margins (Fig. 11). Quartz crystals in the studied samples are variable in size and shapes, and mostly identified within clay aggregates. Therefore, quartz is mainly syngenetic (detrital) in origin. The cavity-infilling silica is rarely observed in the studied samples, and also cleat-infilling epigenic silica is determined in few samples from the Eynez sector. ~~Noteworthy~~It is noteworthy that~~,~~ silica glass shards are also identified during SEM studies where Opal/CT is traced by XRD. The silica shards are generally reported as volcanic inputs (e.g. air-fall ash) from synchronous volcanic activity (Ruppert and Moore, 1993; Karayiğit et al., 2001). Considering these shards and the existence of several ash layers within kM2 and kP1, silicate minerals along apatite, zircon, Ti-oxides and monazite are mainly volcanic inputs during peat accumulation and lesser clastic inputs from margins.

The coal-petrography and SEM data imply that carbonate minerals display variable mode of mineralisation in the examined coal samples. Syngenetic authigenic calcites are the most common carbonate minerals and to a less extent detrital calcites. Cell- and void-infilling together with replacement carbonates are also commonly identified samples from the kM2 seam

(Fig. 10). The gastropod fossil rich bands are generally reported from Turkish Neogene coal deposit; however, aragonite is either in trace amounts or absent on XRD (Querol et al., 1999; Karayiğit et al., 2001, 2015; Oskay et al., 2016). It is normal that aragonite can easily convert to calcite during burial; consequently, aragonite is absent and calcite is the predominant mineral in most of the gastropod-bearing samples in kM3 and kP1 seams. The syngenetic calcites are either individual body and/or commonly associated with siderite nodules (Figs. 10 and 11). Siderites display three crystallization types in the studied samples: Mg-and Mn-bearing Ca-siderites (most common ~~one~~), individual siderite nodules with Mn traces, and siderites associated with dolomite. Siderites in the kP1 seam are generally smaller nodules, whereas larger ones are observed in the coal beds of the kM2 seams (Fig. 11). These siderite nodules are presumably related to the low sulphate contents of ~~influence~~ water flowing into the palaeomire (Ward, 2016; Zhao et al., 2016); however, the total S contents are slightly high in kM3 and kP1 seams and also siderites were commonly identified around pyrite crystals (Fig. 11c). Therefore, siderite might be formed as reactions between iron and dissolved CO_2 in the palaeomire and as well as pore waters. This can ~~example~~ also explain the presence of siderites within the cavities of macerals (Figs. 3c and 11a). Furthermore, leached waters from calcareous intercalations and particularly tuff layers could ~~be~~ penetrate~~d~~ into coal beds during coalification. As a result, reactions between siderite and these solutions, associated with calcite and dolomite or *vice versa* siderites around pyrites, calcite and/or dolomites were formed (Fig. 11).

Pyrite is the only sulphide minerals determined in the XRD traces of the coal samples (Table 5); however, other sulphide minerals were identified by SEM-EDX studies (Fig. 12). Pyrites are mostly represented by syngenetic framboidal crystals and lesser extent epigenetic pyrites (e.g. pyritized macerals and cleat-infilling). Sphalerite and chalcopyrite along with barite are mostly identified in coal beds below the tuff layers and this observation suggests that these were formed from precipitation of leached fluids from those tuff layers. Gypsum was presumably formed by the pore water evaporation during the storage of coal samples.

4.6 Elemental concentration and modes of occurrence

The major elements (≥1000 ppm) in the three seams are Al, Ca, Fe, K, Mg and Na (Table 6). The concentrations of elements like B, P and Ti can reach more than 1000 ppm in some coal samples (Table 6). The concentrations of Ba, Sr, V and Zn are variable in the three seams and these elements can exceed ~~also~~ more than 100 ppm in certain coal samples. In addition, the concentrations of Mn exceeds more than 100 pm in kM2 and kP1 seams. The concentrations of

trace elements are mostly below 10 ppm; however, As and Zr exceed more than 100 ppm in some coal beds below the tuff layers. The previous studies also reported similar elemental concentrations from the feed~~ing~~ coals in the Soma Basin (Karayiğit et al., 2000, 2006; Tuncalı et al., 2002). The vertical distributions of elements are also changeable from seam to seam. The major elements (Al, Fe, K, Mg and Na), and most of minor (e.g. Ba, P, Ti) and trace elements (e.g. Cu, Zn) display increase trends upwards in the kP1 seam, whereas Ca, As and Mo decrease. In contrast, elements tend to decrease towards the~~o~~ upper parts in kM2 and kM3 seams. Boron in the kM2, and Mo and Ba in the kM3 seam display increasing trends ~~to the~~ upwards. These changes are mostly in parallel with the vertical distributions of ash yields in the seams.

The weighted averages of elements in each sector are variable and elemental enrichments are generally changeable (Table 6). Nevertheless, the elements Cs, Li and U are the only enriched elements in almost all the studied coal seams in comparison with ~~the~~ most world coals (Swaine, 1990). In the Deniş sector, B, Cd, Li and V are enriched in both kM2 and kP1 seams, whereas Ti, Cr, and Th are only enriched in the kP1 seam in this sector (Table 6). The elemental concentrations, beside U, in the kM2 seam at the Işıklar sector are within the averages of most world coals, while only Cs, Li and V are enriched in the kM3 seam. In the Eynez sector only Cs and U display enrichments. Furthermore, the concentrations of several minor and trace elements in the three coal seams show higher average values than the world brown coals (Ketris and Yudovich, 2009). The difference between elemental enrichments along with vertical distributions could be related to ash yields. The kM2 seam displays generally lower elemental concentrations and ash yields, in contrast higher elemental concentrations and ash yields were recorded from the kP1 seam (Table 6). Therefore, almost all elements display strong positive correlations between ash yields and strong negative correlation with TOC (Table 7). All ~~these~~ this suggests that s majority of elements mostly have inorganic affinity. Nevertheless, no significant correlation between ash yields and elements such as Ca, As, B, Mo, Se, W and U are recorded. Thus, these elements seem to have an intermediate affinity.

The major elements Al, Fe, K, Mg and Na have strong positive correlations with most of minor and trace elements (Table 7). Considering these correlations along with the common presences of aluminosilicate minerals, Al, Fe, K, Mg and Na and associated elements (e.g. Co, Cr, Li and Zr) are mainly affiliated with clay minerals and/or feldspars in the coal samples. Therefore, clastic inputs from volcanic rocks on the margins might have been the main source of major elements and as well as aluminosilicate affiliate elements. Calcium has only a weak correlation with Sr and this association could be related to the existence of carbonate minerals.

Furthermore, the SEM-EDX data shows that Fe, Mg and Mn are partly derived from carbonate minerals, particularly from siderites (Fig. 11), and also Ca traced from organic matter in the studied coal samples. Overall Ca has an intermediate affinity in the studied samples.

The SEM-EDX data also denoted that minor and trace elements could have another mineral affinity rather than aluminosilicates. The clay mineral aggregates associated with accessory minerals such as zircon, chromite, apatite and monazite that are sources for Zr, P and Cr along with the REEs in the studied samples. The geochemical analyses from volcanic rocks on the margins show the presence of Ba, Cr, Ni, Sr, Zr, Th, U and as well as REEs (Ersoy et al., 2012). These could be evidence that most of minor and trace elements are mostly derived from clastic inputs. Barite could also be the source for Sr (Fig. 12). The elements As, Cu, Pb and Zn were commonly traced from sulphide minerals (Fig. 12), and as mentioned previously, they generally display higher concentrations below the ash layers. This implies that leached waters from tuff layers precipitated within the coal beds during late diagenetic stages. Thus, epigenetic sulphide minerals could cause the As, Cu and Zn enrichments in the kM2 and kP1 seams. The synchronous volcanic activity also caused ~~also~~ B enrichments in most Turkish coals (Querol et al., 1997; Karayiğit et al., 2000). The leached surface waters from volcanic rocks on the margins and tuff layers within the basin could bring B-rich waters into palaeomires in the Soma Basin. Thus, B could uptake by either peat-forming plants or adsorbed by clay minerals. This could explain the intermediate affinity of B in the studied coal samples.

5. Discussion

5.1 Hydrocarbon source potential

The humic coals with high vitrinite/huminite contents with liptinite contents more than 10-15% (on mineral matter-free basis) are generally considered as oil-prone (Hunt, 1991; Snowdon, 1991; Wilkins and George, 2002). Nevertheless, the oil generation potential of humic coals is a complex process and~~,~~ several parameters and diagrams were proposed for accurate interpretations (Pepper and Corvi, 1995; Killops et al., 1998; Sykes and Snowdon, 2002; Petersen, 2006). The huminite and liptinite contents along with thickness of coal beds in the studied coal seams might suggest a possible oil-generation potential (see Table 1 and Fig. 2). The hydrocarbon generation potential of the coal samples is firstly evaluated on HI *vs*. OI and HI *vs*. T_{max} diagrams (Fig. 4). The plot~~ting~~ed data shows that the samples are located on the mainly mixed and gaseous hydrocarbon generation window, which is also consistent with their T_{max} values. The existence of exsudanites in some samples can also suggest the development of

~~the~~ early petroleum generation and the mixed hydrocarbon generation potential for certain coal beds in the Soma Basin. Furthermore, the coals with HI lower than 150 mg HC/g TOC are generally considered as gas-prone (Hunt, 1991; Peters and Moldowan, 1993; Petersen, 2006); thus, investigated samples are more gas-prone rather than mixed generation potential. In addition, several studies also denoted that HI values ~~could~~ are not accurate for humic coals to estimate the true generation potential (Petersen, 2002 and refs. therein), and calculated HI_{max} values (or "effective HI" of Sykes and Snowdon, 2002) on HI *vs.* VR plots could be more accurate for initial hydrocarbon potential. The calculated HI_{max} values are within the range for gas- and oil-prone coals (Fig. 5); and none of sample reach required HI_{max} value (300 mg HC/g TOC) for the oil generation (Fig. 13). Considering this along with $\%R_o$ ($\leq$0.50), low PI, BI and QI values (see Table 1) point that the coal beds in the studied sectors are generally gas-prone.

5.2. Coal facies indices

The coal maceral diagrams could be useful tools when combined~~g~~ with mineralogical, sedimentological, paleontological and geochemical data for providing information about depositional conditions and predominant vegetation within the palaeomire (Bechtel et al., 2014; Karayiğit et al., 2015, 2016). The most widely using ternary diagram, proposed by Mukhopadhyay (1989), provides information about depositional conditions and common vegetation during peat accumulation (Fig. 14). Plotting the data ~~points~~ shows that precursor peat of the kM2 seam accumulated under slight anoxic conditions where the water-table was high and stable. Forested fen was common and good tissue preservation developed. In contrast, the water-table was unstable during peat accumulation in the kM3 and kP1 seams. The dominant vegetation in these seams was herbaceous, particular reed plants. The samples of upper parts of kM3 from Işıklar field display more oxic conditions and inertinite contents are higher than other samples of kM2 ones from the same sector. This difference might be related either drier conditions on this part of the basin or a masking effect from high allocthonous inertinite input. The latter one seems to be more possible due to the predominance of inertodetrinite embedded within densinites. Such association generally indicates allocthonous origin for inertinites rather oxidation (O'Keefe et al., 2013).

The differences between seams are more distinct on the tissue Preservation Index (TPI) *vs.* gelification index (GI) and groundwater influence (GWI) *vs.* vegetation index (VI) diagrams (Fig. 15). The kM2 seam is characterized by high to very high TPI (1.5-16), VI (0.8-5.6), and moderate to high GI (2.2-67.9) values. The TPI-GI values similar with Seam kM2 are generally

reported from xylite-bearing Neogene coal deposits that assess wet swamp to piedmont conditions (Kolcon and Sachenhofer, 1999; Kalaitzidis et al., 2004; Oikonomopolou et al., 2015). The fossilized wood trunks and branches in the kM2 seam is ~~another testimony~~further evidence for the predominance of woody vegetation and wet swamp conditions. The organic geochemistry data also revealed the presence of high plants and the previous palynological studies also imply the dominance of woody vegetation in the basin (Nebert, 1978; Akgün et al., 1986; Gemici et al., 1991). The wet conditions during the kM2 seam could be related to humid climate during late Early to Middle Miocene in ~~the~~ western Turkey (Kayseri-Özer, 2016). The GWI values of the kM2 seam could be interpreted as low water table conditions (Fig. 15). Nevertheless, these low GWI values are characteristic for the Tertiary xylite-rich coals ~~in~~ elsewhere (Kalaitzidis et al., 2004; Koukouzas et al., 2010; Oikonomopoulos et al., 2015; Mitrović et al., 2016). Thus, these low GWI in the kM2 seam can be expected. The low TPI (<1.0) and VI (<1.0), and as well low to moderate GI (0.8-25.4) and GWI (1.6-11.1) values from seams kM3 and kP1 indicate the predominance of herbaceous vegetation and ~~fluctuated~~ fluctuating water-table during peat accumulation (Fig. 15). The *n*-alkane distribution pattern of analysed samples from the kP1 seam also indicates the predominance of the herbaceous (e.g. macrophytes) in the palaeomire. The vegetation difference is presumably related to the changes on climatic conditions and/or depositional environment in the Soma Basin during the Miocene.

5.3. Depositional environment

The Soma Basin ~~is~~ started to form during the Early Miocene as a result~~s~~ of the regional extensional tectonic regime in the western Turkey. The basinal infillings commenced with alluvial deposits, and were followed by fluvial and lacustrine sediments (Nebert, 1978; İnci, 1998a, 2002). Within the development of optimal climatic conditions and clastic input ratio during late Early to early Middle Miocene, the suitable condition for the precursor peat-accumulation of the kM2 and kM3 seams in the Soma Formation was developed in the basin (Takahashi and Jux, 1991; Akgün, 1993; İnci, 2002). The coal facies, lithological and mineralogical data imply that the depositional environment ~~was~~ changed during Soma Formation deposition~~ed~~. The coal facies diagrams suggest the precursor peat of kM2 seam was accumulated under wet forest swamp and piedmont plain (Fig. 15). The seam displays thick coal beds with thin inorganic intercalations also suggesting high and stable water tables and low clastic input ratio. Therefore, coal samples of the kM2 seam display low concentrations of aluminosilicate affiliated elements and TOC values are higher. The latter one also supports the authochthonous peat formation. The low energy and high water table conditions are also

favourable for gelification and pyrite formation (Siavalas et al., 2009; Oikonomopolou et al., 2015). Therefore, syngenetic pyrites are commonly observed. In addition, low energy conditions allowed precipitation of siderites in the palaeomires (Oikonomopolou et al., 2008) and larger siderites nodules in the kM2 seam presumably formed in such a way. Their co-existence with other syngenetic carbonates and pyrites also imply neutral to weak alkaline conditions during peat accumulation. Furthermore, the predominance of woody vegetation and better preservation conditions are generally relating to high HI values (Collinson et al., 1994; Petersen et al., 2009) and this relation might explain slightly higher HI and as well as TOC values in the kM2 seam (see Table 1). The extensional tectonic regime during the Early to Middle Miocene ~~caused~~ also caused the development of volcanic activity (Seyitoğlu and Scott, 1996; Ersoy et al., 2014); hence, several tuff layers, altered volcanic materials, pyroclastic and volcanoclastic material were identified within coal seams and lacustrine sediments of the Soma Basin (Karayiğit, 1998; İnci, 1998b; 2002). Therefore, peat accumulation seems to ~~be~~ cease~~d~~ only by regional volcanic activities that resulted in the tuff layers in the kM2 seam, and the silicate minerals in this seam are mainly derived from these tuff layers and lesser amount brought by sheetwash/runoffs from margins.

The clayey limestone/marl that was previously identified as a marl series by İnci (1998a, 2002) forms the roof rock of the kM2 seam. This unit is related to the development of deeper conditions and/or lake expansion in the Soma Basin as a result vertical tectonic movements. Furthermore, the presence of clay minerals in this unit also indicates that the clastic inputs by ~~fluival~~fluvial systems were also developed during this period ~~of time~~. With the development of shallow conditions, the precursor peat of kM3 ~~was~~ started to accumulate; ~~nevertheless,~~ the peat-accumulation ~~was~~ ceased several times and calcareous intercalations were deposited (Fig. 2). This alteration between coal beds and calcareous intercalations could be the indicator for vertical tectonic movements that presumably activated karstic aquifers on the margins. Therefore, Ca-rich water discharge into the basin was increased and such discharges generally resulted in development of alkaline conditions in the palaeomire (Bechtel et al., 2004; Siavalas et al., 2009; Karayiğit et al., 2015). As a result, carbonate minerals and fossil fragments are common in the kM3 seam and Ca concentrations are higher than the kM2 seam. The existence of syngenetic pyrites in this seam also implies~~y~~ the influence of SO_4^{2-}-rich water into the palaeomire and the development of neutral to weak alkaline conditions. Furthermore, the development of alkaline conditions also allows ~~the~~ bacterial activity that could reduce tissue preservation, and this also explains relatively low TOC and TPI values in this seam. These

values might also be related to the predominance of herbaceous vegetation in the palaeomire. During early the Middle Miocene, climatic condition ~~seems~~ appears to be changed and forested vegetation turned to herbaceous, particularly reed species. Overall, the precursor peats in the Soma Formation started to accumulated under pure telmatic conditions at the early stages of peat accumulation (kM2 seam), whereas limno-telmatic conditions are ~~being~~ more dominant in the late stages of peat accumulation (kM3 seam) in this ~~formation~~Formation.

~~Within~~ At the start of the Late Miocene, fluvial conditions were again ~~being~~ dominant and these conditions turned to limnic conditions where the precursor peat of the kP1 seam was accumulated. On the lower parts of the kP1 seam calcareous intercalations and fossil shell-remains are common and thus carbonate minerals are the dominant phase, whereas coal beds with clay-bands are also common on the upper parts. These differences on mineralogical, lithological and maceral compositions of coal beds throughout the kP1 seam suggest changes ~~on~~ in water chemistry ~~of water~~ in the palaeomire and clastic input ratios during the Late Miocene. The lower parts were presumably deposited in alkaline conditions and low clastic input ratio that allowed the formation of syngenetic carbonates. The predominance of silicates along with high ash yields on the upper parts imply the tectonic movements and increased clastic input ratio into the basin. Moreover, ~~the~~ regional volcanic activity took place again during Late Miocene around the Soma Basin (İnci, 1998b, Ersoy et al., 2012); thus, an altered tuff layer was also identified in the kP1 seam (see Fig. 2). ~~Noteworthy,~~It is noted that clayey bands and silicate minerals are ~~being~~ dominant above this layer and this suggests that the clastic input ratio from margins was increased after the volcanic activity during the Late Miocene. The concentrations of aluminosilicate affiliated minerals are consequently elevated towards to upper parts of the kP1 seam. The increased clastic inputs along with alkaline conditions could also reduce preservation of organic matter that resulted in lower TOC values in this seam. All these denote the peat accumulated under limno-telmatic condition where fluvial and volcanoclastic inputs ceased peat formation several times during the Late Miocene.

6. Summary and conclusions

The alternations between alluvial-fluvial-lacustrine conditions imply the Soma Graben was activated several times during the Miocene as a result of the regional extensional tectonic regime. This regime together with climatic factors controlled peat-forming environment in the Soma Basin and effected the ~~coal~~ quality of the coal seams. The palaeomire in the Soma Basin commenced to develop under pure telmatic and low energy conditions and peat-forming

vegetation was dominated by woody species. This condition resulted in the formation of thick coal beds, low ash yields and high TOC values in the kM2 seam. ~~Following~~ Over following periods the~~,~~ water-table fluctuated several times and covered the entire mire surface; thus, peat formation ceased several times that resulted in the deposition of clastic and calcareous intercalations in kM3 and kP1 seams. The lithological and mineralogical features of these intercalations indicate the development of limno-telmatic conditions with fluvial contributions during accumulation of precursor peats of the kM3 and kP1 seams. Furthermore, the ~~inundated~~ inundating water into the palaeomire was presumably Ca-rich and shifts to more alkaline conditions in the palaeomires within the basin. Therefore, coal samples of the kM3 and kP1 seams display relatively high total S contents and low TOC values. Another important result of extensional tectonic regime is the formation of volcanic activity during the precursor peats accumulation of kM2 and kP1 seams; hence, several altered tuff layers were identified within these seams. The mineralogical compositions of these layers also ~~point~~ indicates that these were originated from felsic volcanic activities around the Soma Basin and ~~also~~ their compositions are similar to tonsteins. Thus, these layers are presumably ~~in~~ of air-fall ash origin.

The results of the pyrolysis analysis of the coal samples are in agreement with maceral compositions and rank. The kerogen type-III is common in the all seams and low OI values in the kM3 are related to slightly high inertinite values. The HI and T_{max} values ~~point~~ indicate that samples from the kM2 and kM3 seams are immature to early mature and from the kP1 seam are clearly immature. Furthermore, the changes i~~o~~n vegetation during the Miocene in the Soma Basin also have ~~reflections~~ influences on the HI values. The slightly higher HI in the kM2 seems to be related to high contributions of woody material in the peat and development of more acidic conditions during peat-accumulation, whereas relative low HI values in kM3 and kP1 are related to contributions of herbaceous plants and more alkaline conditions. Even though, the thickness of coal beds along with high huminite and liptinite contents of the coal samples ~~can~~ suggests the oil generation potential, the pyrolysis analysis data shows that studied coal seams are mainly gas-prone and only certain coal beds have mixed hydrocarbon generation capacity. All these suggest the features of coals seams were in the Soma Basin were controlled by changes on the depositional conditions and vegetation during the Miocene.

Acknowledgements

This study is supported under the grants of 00.02.602.005 and FAY-201-10601 projects by the Scientific Research Coordination Unit of the Hacettepe University. The first author is also

would like to thank to the German Academic Exchange Service (DAAD) for granting of the research visits during the project. The authors also would to thank Prof. Dr. İsmail Hakkı Demirel (Hacettepe University), Asst. Prof. Dr. İbrahim Buzkan (Bülent Ecevit University), Dr. Maria Mastalerz (Indiana University) for their helps and suggesting during the project. Finally, Dr. Oskay would like express his gratitude to Department of Geology, Hacettepe University for the hospitality during research visit.

References

American Society for Testing and Materials (ASTM) D3174, 2012. Standard Test Method for Ash in the Analysis Sample of Coal and Coke from Coal, ASTM International, West Conshohocken, PA, 6 pp.

American Society for Testing and Materials (ASTM) D5865, 2013. Standard Test Method for Gross Calorific Value of Coal and Coke, ASTM International, West Conshohocken, PA, 19 pp.

American Society for Testing and Materials (ASTM) D3302, 2015. Standard Test Method for Total Moisture in Coal, ASTM International, West Conshohocken, PA, 8 pp.

American Society for Testing and Materials (ASTM) D5373, 2016. Standard Test Methods for Determination of Carbon, Hydrogen and Nitrogen in Analysis Samples of Coal and Carbon in Analysis Samples of Coal and Coke, ASTM International, West Conshohocken, PA, 11 pp.

Akgün, F., 1993.Palynological age revision of the Neogene Soma Coal Basin. *Bull. Geol. Soc. Greece* 28, 151–170.

Akgün, F., Alişan, C., Akyol, E., 1986.A palynological approach to the Neogene Stratigraphy of Soma area. *Geol. Soc. Turk. Bull.* 29, 13-25.

Arbuzov, S.I., Mezhibor, A.M., Spears, D.A., Ilenok, S.S., Shaldybin, M.V., Belaya, E.V., 2016. Nature of tonsteins in the Azeisk deposit of the Irkutsk Coal Basin (Siberia, Russia). *Int. J. Coal Geol.* 153, 99-111.

Baysal, M., Yürüm, A., Yıldız, B., Yürüm, Y., 2016.Structure of some western Anatolia coals investigated by FTIR, Raman, ^{13}C solid state NMR spectroscopy and X-ray diffraction. *Int. J. Coal Geol.* 163, 166-176.

Bechtel, A., Markic, M., Sachsenhofer, R.F., Jelen, B., Gratzer, R., Lücke, A., Püttmann, W., 2004. Paleoenvironment of the upper Oligocene Trbovlje coal seam (Slovenia). *Int. J. Coal Geol.* 57, 23-48.

Bechtel, A., Karayiğit, A.İ., Sachsenhofer, R.F., İnaner, H., Christanis, K., Gratzer, R., 2015. Spatial and temporal variability in vegetation and coal facies as reflected by organic petrological and geochemical data in the Middle Miocene Çayirhan coal field (Turkey). *Int. J. Coal Geol.* 134–135, 46–60.

Benda, L., 1971. Principles of the palynologic subdivision of the Turkish Neogene. *Newsl. Stratigr.* l, 23-26.

Bohor, B.F., Triplehorn, D.M., 1993. Tonstein: altered volcanic ash layers in coal-bearing sequences. *Geol. Soc. of Am. Spec. Paper* 285, 40.

Bulut, Y., Karayiğit, A.İ., 2006. Petrography of feed coals in the Soma Power Plant, Manisa, Turkey. *Energy Sources, Part A* 28, 1447–1459.

Burger, K., Bandelow, F.K., Bieg, G., 2000. Pyroclastic kaolin coal–tonsteins of the Upper Carboniferous of Zonguldak and Amasra, Turkey. *Int. J. Coal Geol*. 45, 39-53.

Burger, K., Zhou, Y., Ren, Y., 2002. Petrography and geochemistry of tonsteins from the 4th Member of the Upper Triassic Xujiahe formation in Southern Sichuan Province, China. *Int. J. Coal Geol*. 49, 1-17.

Calder, J., Gibling,M., Mukhopadhyay, P., 1991. Peat formation in a Westphalian B piedmont setting, Cumberland Basin, Nova Scotia. *Bull. Soc. Géol. Fr.* 162, 283–298.

Canuel, E., Freeman, K., Wakeham, S., 1997. Isotopic compositions of lipid biomarker compounds in estuarine plants and surface sediments. *Limnol. Oceanogr.* 42, 1570–1583.

Collinson, M.E., Van Bergen, P.F., Scott, A.C., De Leeuw, J.W., 1994. The oil-generating potential of plants from coal and coal-bearing strata through time: a review with new evidence from Carboniferous plants. In: Scott, A. C., and Fleet, A. J. (eds.) Coal and coal-bearing strata as oil-prone source rocks?. *Geol. Soc. London, Spec. Publ.* 77, 31-70.

Dai, S., Wang, X., Zhou, Y., Hower, J.C., Li, D., Chen, W., Zhu, X., Zou, J., 2011. Chemical and mineralogical compositions of silicic, mafic, and alkali tonsteins in the late Permian coals from the Songzao Coalfield, Chongqing, Southwest China. *Chem. Geo.* 282, 29-44.

Diessel, C.F.K., 1992. Coal-bearing depositional systems. Springer, Berlin, 721 pp.

Ersoy, E., Dindi, F., Karaoğlu, O., Helvacı, C., 2012. Geochemical and Petrographic Features of the Miocene Volcanism Around Soma Basin, Western Anatolia, Turkey. *Yerbilimleri* 33, 59-80 (in Turkish with English abstract).

Escobar, M., Márquez, G., Suárez-Ruiz, I., Juliao, T.M., Carruyo, G., Martínez, M., 2016. Source-rock potential of the lowest coal seams of the Marcelina Formation at the Paso Diablo mine in the Venezuelan Guasare Basin: Evidence for the correlation of Amana oils with these Paleocene coals. *Int. J. Coal Geol*. 163, 149-165.

Espitalié, J., Laporte, J.L., Madec, M., Marquis, F., Leplat, P., Paulet, J., Boutefeu, A., 1977a. Méthode rapide de caractérisation des roches mères de leur potentiel pétrolier et de leur degré d'évolution. *Revue de L'Institut Français du Pétrole* 32, 23–42.

Espitalié, J., Madec, M., Tissot, B., 1977b. Source rock characterization method for petroleum exploration. Proceedings 9th Offshore Technology Conference Vol. 3, Houston, 439–444.

Ficken, K.J., Li, B., Swain, D.L., Eglinton, G., 2000. An n-alkane proxy for the sedimentary input of submerged/floating freshwater aquatic macrophytes. *Org. Geochem.* 31, 745–749

Gemici, Y., Akyol, E., Akgün, F., Seçmen, Ö., 1991. Macro and micro fossil flora of Soma coal area. *Bull. of the Min. Res. and Expl*.112, 161-178 (in Turkish with English abstract).

Gross, D., Bechtel, A., Harrington, G.J., 2015. Variability in coal facies as reflected by organic petrological and geochemical data in Cenozoic coal beds offshore Shimokita (Japan) - IODP Exp.337. *Int. J. Coal Geol*. 152, 63-79.

Hokerek, S.,Ozcelik, O., 2015.Organic facies characteristics of the Miocene Soma Formation (Lower Lignite Succession-KM2), Soma Coal Basin, western Turkey. *Energy Procedia* 76, 27-32.

Hunt, J.M., 1991. Generation of gas and oil from coal and other terrestrial organic matter. *Org. Geochem.* 17, 673–680.

International Committee for Coal Petrology (ICCP), 1994. The new vitrinite classification (ICCP System 1994). *Fuel* 77, 349–358.

International Committee for Coal Petrology (ICCP), 2001. The new inertinite classification (ICCP System 1994). *Fuel* 80, 459–471.

International Standard Organisation (ISO) 11760, 2005. Classification of coals. International Organization for Standardization, Geneva, Switzerland, 9 pp.

International Standard Organization (ISO) 7404–2, 2009. Methods for the petrographic analysis of coals — part 2: methods of preparing coal samples. International Organization for Standardization, Geneva, Switzerland, 12 pp.

International Organization for Standardization (ISO) 7404–5, 2009. Methods for the petrographic analysis of coal —Part 5: method of determining microscopically the reflectance of vitrinite. International Organization for Standardization, Geneva, Switzerland, 14 pp.

İnci, U., 1998a. Lignite and carbonate deposition in middle lignite succession of the Soma Formation, Soma coalfield, western Turkey. *Int. J. Coal Geol*. 37, 287–313.

İnci, U., 1998b. Miocene synvolcanic alluvial sedimentation in Lignite-bearing Soma Basin, Western Turkey. *Turk. J. Earth Sci.*7, 63-78.

İnci, U., 2002. Depositional evolution of Miocene coal successions in the Soma coalfield, western Turkey. *Int. J. Coal Geol*. 51, 1–29.

Kalaitzidis, S., Bouzinos, A., Papazisimou, S., Christanis, K., 2004. A short-term establishment of forest fen habitat during Pliocene lignite formation in the Ptolemais Basin, NW Macedonia, Greece. *Int. J. Coal Geol.* 57, 243-263.

Kalaitzidis, S., Siavalas, G., Skarpelis, N., Araujo, C.V., Christanis, K., 2009. Late Cretaceous coal overlying karstic bauxite deposits in the Parnassus-Ghiona Unit, Central Greece: Coal characteristics and depositional environment. *Int. J. Coal Geol.* 81, 211-226.

Karayiğit A.İ., 1998. Thermal effects of a basaltic intrusion on the Soma lignite bed in west Turkey. *Energy Sources* 20, 55-66.

Karayiğit, A.İ., Whateley, M.K.G., 1997. Properties of a lacustrine subbituminous (kl) seam, with special reference to the contact metamorphism. Soma-Turkey. *Int. J. Coal Geol*.34, 131-155.

Karayiğit, A.I., Gayer, R.A., Querol, X., Onacak, T., 2000. Contents of major and trace elements in feed coals from Turkish coal-fired power plants. *Int. J. Coal Geol.* 44, 169-184.

Karayiğit, A.I., Gayer, R.A., Ortac, F. E., Goldsmith, S., 2001. Trace elements in the Lower Pliocene fossiliferous Kangal lignites, Sivas, Turkey. *Int. J. Coal Geol.* 47, 73-89.

Karayiğit , A.I., Bulut, Y., Querol, X., Alastuey, A., Vassilev, S., 2006. Variations in fly ash composition from the Soma Power Plant, Turkey. *Energy Sources* 27, 1473-1481.

Karayiğit, A.I., Oskay, R.G., Christanis, K., Tunoğlu, C., Tuncer, A., Bulut, Y., 2015. Palaeoenvironmental reconstruction of the Çardak coal seam, SW Turkey. *Int. J. Coal Geol.* 139, 3-16.

Kayseri-Özer, S., 2017. Cenozoic vegetation and climate change in Anatolia -A study based on the IPR-vegetation analysis. *Palaeogeogr. Palaeoclimatol. Palaeoecol.* 467, 37-68.

Ketris, M.P., Yudovich, Ya.E., 2009. Estimations of Clarkes for carbonaceous biolithes: world averages for trace element contents in black shales and coals. *Int. J. Coal Geol.* 78, 135–148.

Kolcon, I., Sachsenhofer, R.F., 1999. Petrography, palynology and depositional environments of the early Miocene Oberdorf lignite seam (Styrian Basin, Austria). *Int. J. Coal Geol.* 41, 275-308.

Koukouzas, N., Kalaitzidis, S.P., Ward, C.R., 2010. Organic petrographical, mineralogical and geochemical features of the Achlada and Mavropigi lignite deposits, NW Macedonia, Greece. *Int. J. Coal Geol.* 83, 387-395.

Mukhopadhyay, P., 1989. Organic Petrography and Organic Geochemistry of Tertiary Coals from Texas in Relation to Depositional Environment and Hydrocarbon Generation. Report of Investigations, Bureau of Economic Geology, Texas, 118 pp.

Nebert, K. 1978. Das braunkohlenführende Neogengebiet von Soma, Westanatolien. *Bull. of the Min. Res. and Expl.* 90, 20-72.

Oikonomopoulos, I., Kaouras, G., Antoniadis, P., Perraki, T., Gregor, H.-J., 2008. Neogene Achlada lignite deposits in NW Greece. *Bull. of Geosci.* 83, 335-349.

Oikonomopoulos, I.K., Kaouras, G., Tougiannidis, N., Ricken, W., Gurk, M., Antoniadis, P., 2015. The depositional conditions and the palaeoenvironment of the Achlada xylite-dominated lignite in western Makedonia, Greece. *Palaeogeogr. Palaeoclimatol. Palaeoecol.* 440, 777-792.

O'Keefe, J.M.K., Bechtel, A., Christanis, K., Dai, S., Di Michele, W.A., Eble, C.F., Esterle, J.S., Mastalerz, M., Raymond, A.L., Valentim, B.V., Wagner, N.J., Ward, C.R., Hower, J.C., 2013. On the fundamental difference between coal rank and coal type. *Int. J. Coal Geol.* 118, 58–87

Oskay, R.G., Christanis, K., İnaner, H., Salman, M., Taka, M., 2016. Palaeoenvironmental reconstruction of the eastern part of the Karapınar-Ayrancı coal deposit (Central Turkey). *Int. J. Coal Geol.* 163, 100-111.

Querol, X., Fernández-Turiel, J.; López-Soler, A., 1995. Trace elements in coal and their behaviour during combustion in a large power station. *Fuel* 74, 331-343.

Querol, X., Whateley, M.K.G., Fernández-Turiel, J.L., Tuncalı, E., 1997. Geological controls on the mineralogy and geochemistry of the Beypazari lignite, central Anatolia, Turkey. *Int. J. Coal Geol.* 33, 255-271.

Querol, X., Alastuey, A., Plana, F., Lopez-Soler, A., Tuncali, E., Toprak, S., Ocakoglu, F., Koker, A., 1999. Coal geology and coal quality of the Miocene Mugla basin, southwestern Anatolia, Turkey. *Int. J. Coal Geol.* 41, 311-332.

Palmer, C.A., Tuncalı, E., Dennen, K.O., Coburn, T.C., Finkelman, R.B., 2004. Characterization of Turkish coals: a nationwide perspective. *Int. J. Coal Geol.* 60, 85-115.

Peters, K.E., 1986. Guidelines for evaluating petroleum source rock using programmed pyrolysis. *AAPG Bull.* 70, 318–329.

Peters, K.E., Moldowan, J.M., 1993. The Biomarker Guide: Interpreting Molecular Fossils in Petroleum and Ancient Sediments. Prentice Hall, Englewood Cliff, 363 pp.

Petersen, H.I., 2002. A re-consideration of the "oil window" for humic coal and kerogen type III source rocks. *J. Pet. Geol.* 25, 407–432.

Petersen, H.I., Rosenberg, P., 2000. The relationship between the composition and rank of humic coals and their activation energy distributions for the generation of bulk petroleum. *Petrol. Geosci.* 6, 137-149.

Petersen, H.I., Lindström, S., Nytoft, H.P., Rosenberg, P., 2009. Composition, peat-forming vegetation and kerogen paraffinicity of Cenozoic coals: Relationship to variations in the petroleum generation potential (Hydrogen Index). *Int. J. Coal Geol.* 78, 119-134.

Pickel, W., Kus, J., Flores, D., Kalaitzidis, S., Christanis, K., Cardott, B.J., Misz-Kennan, M., Rodrigues, S., Hentschel, A., Hamor-Vido, M., Crosdale, P., Wagner, N., 2017. Classification of liptinite – ICCP System 1994. *Int. J. Coal Geol.* 169, 40-61.

Ruppert, L.F., Moore, T.A., 1993. Differentiation of volcanic ash-fall and water-borne detrital layers in the Eocene Senakin coal bed, Tanjung Formation, Indonesia. *Org. Geochem.* 20, 233-247.

Seyitoğlu, G., Scott, B., 1991. Late Cenozoic crustal extension and basin formation in west Turkey. *Geol. Mag.* 128, 155–166.

Seyitoğlu, G., Scott, B., 1996. The cause of N–E extensional tectonics in western Turkey: tectonic escape *vs*. back-arc spreading vs. orogenic collapse. *J. Geodyn.* 22, 145–153.

Siavalas, G., Linou, M., Chatziapostolou, A., Kalaitzidis, S., Papaefthymiou, H., Christanis, K., 2009. Palaeoenvironment of Seam I in the Marathousa Lignite Mine, Megalopolis Basin (Southern Greece). *Int. J. Coal Geol.*78, 233-248.

Spears, D.A., 2012. The origin of tonsteins, an overview, and links with seatearths, fireclays and fragmental clay rocks. *Int. J. Coal Geol.* 94, 22-31.

Swaine, D.J., 1990. Trace Elements in Coal. Butterworths, London, 278 pp.

Sykes, R., Snowdon, L.R., 2002. Guidelines for assessing the petroleum potential of coaly source rocks using Rock-Eval pyrolysis. *Org. Geochem.* 33, 1441-1455.

Sýkorová, I., Pickel, W., Christanis, K., Wolf, M., Taylor, G.H., Flores, D., 2005. Classification of huminite — ICCP System 1994. *Int. J. Coal Geol.* 62, 85–106.

Takahashi, K., Jux, U., 1991. Miocene palynomorphs from lignites of the Soma Basin (west Anatolia, Turkey). *Bull. of the Fac. of Liberal Arts, Nagasaki Unv. Nat. Sci.* 32, 7-165.

Tercan, A.E., Ünver, B., Hindistan, M.A., Ertunç, G., Atalay, F., Ünal, S., Killioğlu, Y., 2013. Seam modeling and resource estimation in the coalfields of western Anatolia. *Int. J. Coal Geol.* 112, 94-106.

Tissot, B.P., Welte, D.H., 1984. Petroleum and formation occurrence. Springer, Berlin, 699 pp.

Toprak, S., 2009. Petrographic properties of major coal seams in Turkey and their formation. *Int. J. Coal Geol.* 78, 263-275.

Tuncalı, E., Çiftci, B., Yavuz, N., Toprak, S., Köker, A., Gencer, Z., Ayçık, H., Pahin, N., 2002. Chemical and Technological Properties of Turkish Tertiary Coals. MTA Publication, Ankara, 401 pp.

Turkish Lignite Company-Aegean Lignite Cooperation (TKİ-ELİ), 2015. The annual report of 2015. Soma-Manisa, Turkey, 23 pp. (accessible at http://www.eli.gov.tr).

Ward, C.R., 2016. Analysis, origin and significance of mineral matter in coal: An updated review. *Int. J. Coal Geol.* 165, 1-27.

Wilkins, R.W.T., George, S.C., 2002. Coal as a source rock for oil: A review. *Int. J. Coal Geol.* 50, 317-361.

Yılmaz Y., Genç, Ş.C., Gürer, F., Bozcu, M., Yılmaz, K., Karacık, Z., Altunkaynak, S.¸Elmas, A., 2000. When did the western Anatolian Grabens begin to develop? In: Bozkurt, E., Winchester, J.A., and Piper, J.A.D. (eds) Tectonics and magmatism in Turkey and the surrounding area. *Geol. Soc. London, Spec. Publ.* 173 131–162.

Vassilev, S.V., Vassileva, C.G., Karayiğit, A.I., Bulut, Y., Alastuey, A., Querol, X., 2005. Phase-mineral and chemical composition of composite samples from feed coals, bottom ashes and fly ashes at the Soma power station, Turkey. *Int. J. Coal Geol*. 61, 35-63.

Volkman, J.K., 1986. A review of sterol markers for marine and terrigenous organic matter. *Org. Geochem.* 9, 83–99.

Zhao, L., Sun, J., Guo, W., Wang, P., Ji, D., 2016. Mineralogy of the Pennsylvanian coal seam in the Datanhao mine, Daqingshan Coalfield, Inner Mongolia, China: Genetic implications for mineral matter in coal deposited in an intermontane basin. *Int. J. Coal Geol*. 167, 201-214.

Table 1
Ranges and weighted averages (in parenthesis) of proximate and ultimate analyses, and Rock-Eval pyrolysis of the coal samples from the Soma Basin (CV: calorific value, TOC: total organic carbon, TIC: total inorganic carbon, HI: hydrogen index, OI: oxygen index, PI: production index; BI: bitumen index, QI: quality index, ar: as received; adb: air-dried basis; db: dry basis; daf: dry, ash-free basis; maf: moist, ash-free basis)

Seam/Sector	kM2			kM3	kP1
	Eynez	Işıklar	Deniş	Işıklar	Deniş
Total Moisture (wt.%, ar)	11.1-17.8 (14.7)	7.5-16.8 (11.8)	13.7-20.7 (18.3)	9.6-14.5 (11.2)	14.4-25.6 (18.7)
Ash (wt.%, db)	3.7-32.3 (16.2)	4.1-37.3 (12.1)	4.2-42.2 (249.6)	14.5-56.9 (36.2)	7.6-64.7 (45.3)
Volatile Matter (wt.%, daf)	42.9-58.7 (54.8)	42.6-55.6 (46.2)	46.4-59.4 (52.1)	46.7-62.2 (56.8)	47.1-67.6 (57.6)
Gross CV (MJ/kg, maf)	22.7-26.5 (24.8)	20.9-27.7 (25.2)	16.2-23.2 (20.6)	18.0-25.0 (21.5)	13.2-21.5 (17.1)
Total S (wt.%, db)	0.4-2.1 (0.8)	0.2-2.0 (1.0)	0.2-1.6 (0.6)	2.4-3.5 (3.1)	0.5-5.0 (1.7)
TC (%, adb)	45.5-64.5 (56.2)	39.3-64.5 (57.3)	34.5-57.6 (43.5)	23.8-55.4 (38.7)	18.5-57.0 (31.7)
TOC (%, adb)	45.4-64.4 (56.0)	38.5-64.3 (56.7)	32.5-57.4 (42.7)	23.4-54.8 (38.0)	17.9-56.9 (31.1)
TIC (%, adb)	0.1-0.5 (0.3)	0.1-2.4 (0.6)	0.2-2.0 (0.7)	0.1-2.1 (0.7)	0.1-4.7 (0.6)
S1 (mg HC/g rock)	1.1-2.4 (1.5)	1.0-3.7 (1.7)	1.2-3.3 (2.3)	0.6-1.2 (0.9)	0.7-1.9 (1.0)
S2 (mg HC/g rock)	62.8-107.2 (83.5)	56.7-103.2 (77.7)	33.7-83.1 (51.7)	35.5-55.5 (43.6)	22.2-71.9 (36.6)
S3 (mg HC/g rock)	7.0-12.1 (10.7)	9.8-15.1 (12.8)	4.5-16.9 (8.6)	7.9-15.1 (10.4)	3.2-19.4 (5.6)
T_{max} (°C)	413-427 (420)	410-426 (418)	392-420 (411)	420-439 (431)	412-430 (424)
HI (mg HC/g TOC)	121-173 (149)	109-178 (137)	88-145 (121)	92-152 (120)	76-142 (120)
OI (mg HC/g rock)	15-20 (19)	21-25 (23)	13-37 (20)	25-34 (28)	14-41 (18)
PI (S1/(S1 + S2)	0.01-0.03 (0.02)	0.01-0.04 (0.02)	0.03-0.05 (0.04)	0.01-0.03 (0.02)	0.02-0.03 (0.03)
BI (S1/TOC)	0.02-0.04 (0.03)	0.02-0.06 (0.03)	0.03-0.07 (0.05)	0.01-0.05 (0.03)	0.02-0.05 (0.04)
QI (S1+S2)/TOC)	1.2-1.8 (1.5)	1.1-1.8 (1.4)	0.9-1.5 (1.2)	0.9-1.5 (1.2)	0.8-1.4 (1.2)

Table 2

Coal-petrography results of the coal samples from the Soma Basin (TH: telohuminite, DH: detrohuminite, GH: gelohuminite, H: huminite. I: inertinite, L: liptinite, MM: mineral matter, SD: standard deviation)

Seam	Sector	Sample	TH	DH	GH	H	L	I	MM	%Ro±SD
			(vol.%. on whole basis)							
kM2	Eynez	E-1	44.4	32.1	8.4	84.9	6.3	1.1	7.7	0.46 ± 0.02
		E-3	37.2	30.6	4.7	72.5	5.5	0.6	21.4	0.46 ± 0.02
		E-5	36.9	28.5	5.5	70.9	6.8	0.2	22.1	0.45 ± 0.02
		E-6	23.0	25.2	3.5	51.7	9.9	0.6	37.8	0.44 ± 0.02
		E-7	48.3	30.8	5.5	84.6	11.4	0.6	3.4	0.44 ± 0.01
		E-8	31.2	17.8	4.1	53.1	7.5	0.8	38.6	0.46 ± 0.02
		E-9	36.3	14.1	2.0	52.4	7.7	2.3	37.6	0.45 ± 0.02
		E-11	35.3	18.8	4.3	58.4	12.3	1.0	28.3	0.44 ± 0.01
		E-11/1	29.7	13.0	3.5	46.2	9.0	0.4	44.4	0.45 ± 0.02
		E-12	35.0	10.0	2.4	47.4	10.3	1.0	41.3	0.45 ± 0.02
		E-13	35.3	15.9	3.1	54.3	8.8	3.3	33.6	0.45 ± 0.03
	Işıklar	I-22	42.3	28.1	10.0	80.4	9.0	0.4	10.2	0.44 ± 0.01
		I-20	49.0	16.9	12.6	78.5	7.4	3.2	10.9	0.44 ± 0.01
		I-19	52.6	17.7	13.3	83.6	7.7	0.4	8.3	0.44 ± 0.01
		I-18	42.2	13.3	6.5	62.0	6.4	0.2	31.4	0.43 ± 0.01
		I-15	46.2	19.6	7.6	73.4	12.4	-	14.2	0.44 ± 0.02
		I-13	37.4	23.2	7.2	67.8	14.0	0.2	18.0	0.42 ± 0.02
		I-12	47.1	13.2	7.4	67.7	9.5	0.6	22.2	0.44 ± 0.01
		I-11	44.6	16.1	5.6	66.3	9.9	0.4	23.4	0.43 ± 0.01
		I-10	18.5	12.5	2.4	33.4	5.4	-	61.2	0.44 ± 0.01
		I-9	55.3	7.8	5.7	68.8	9.0	0.2	22.0	0.44 ± 0.02
		I-8	41.0	12.0	4.5	57.5	10.0	0.6	31.9	0.42 ± 0.01
		I-7	39.3	6.8	4.7	50.8	3.9	0.4	44.9	0.43 ± 0.01
		I-6	33.7	15.2	2.5	51.4	9.8	2.9	35.9	0.43 ± 0.01
		I-4	25.6	12.2	3.3	41.1	7.7	0.4	50.8	0.42 ± 0.01
		I-2	24.4	8.9	3.3	36.6	5.7	0.2	57.5	0.42 ± 0.01
		I-1	41.6	16.2	6.0	63.8	16.9	0.8	18.5	0.43 ± 0.02
	Deniş	D-39	61.2	6.7	9.5	77.4	7.1	-	15.5	0.37 ± 0.02
		D-38	20.9	13.1	2.4	36.4	11.3	0.6	51.7	0.39 ± 0.02
		D-36	25.9	7.5	4.3	37.7	4.8	0.4	57.1	0.39 ± 0.01
		D-35	37.9	17.3	4.7	59.9	9.0	0.2	30.9	0.36 ± 0.02
		D-34	23.8	6.7	3.0	33.5	4.0	-	62.5	0.37 ± 0.02
		D-33	41.9	9.0	6.3	57.2	11.2	-	31.6	0.37 ± 0.01
		D-32	42.7	14.5	7.2	64.4	7.8	0.4	27.4	0.38 ± 0.02
		D-31	39.4	10.7	4.6	54.7	14.3	0.2	30.8	0.38 ± 0.01
		D-29	22.0	18.1	6.4	46.5	6.2	0.2	47.1	0.39 ± 0.02
		D-28	30.0	17.7	5.7	53.4	9.5	-	37.1	0.40 ± 0.02
kM3	Işıklar	I-33	20.0	30.9	10.6	61.5	9.5	10.2	18.8	0.46 ± 0.02
		I-32	7.4	15.3	4.4	27.1	6.9	11.0	55.0	0.45 ± 0.03
		I-31	23.9	37.8	9.7	71.4	7.4	8.9	12.3	0.46 ± 0.02
		I-30	6.7	30.3	2.6	39.6	8.2	5.7	46.5	0.46 ± 0.03
		I-28	20.4	39.0	7.3	66.7	6.1	4.1	23.1	0.45 ± 0.02
		I-27	5.5	32.7	3.3	41.5	6.1	4.9	47.5	0.45 ± 0.03
		I-26	9.4	26.9	3.4	39.7	4.2	5.8	50.3	0.46 ± 0.02
		I-25	4.8	27.6	1.9	34.3	6.5	3.3	55.9	0.46 ± 0.02
		I-24	5.7	7.5	2.3	15.5	5.2	1.2	78.1	0.45 ± 0.02

Table 2 (continued)

		D-25	15.9	10.8	4.1	30.8	4.2	1.8	63.2	0.45 ± 0.02
		D-24	8.7	12.8	3.2	24.7	10.2	0.2	64.9	0.38 ± 0.02
		D-23	3.4	5.6	1.2	10.2	7.5	0.2	82.1	0.40 ± 0.02
		D-22	6.5	7.6	1.4	15.5	6.8	-	77.7	0.41 ± 0.02
		D-21	6.9	12.8	3.3	23.0	3.5	-	73.5	0.41 ± 0.02
		D-18	3.4	4.7	0.5	8.6	6.1	0.4	84.9	0.39 ± 0.02
		D-17	4.4	6.7	2.9	14.0	4.0	0.8	81.2	0.40 ± 0.02
		D-15	13.4	34.9	8.7	57.0	7.6	1.1	34.3	0.40 ± 0.02
kP1	Deniş	D-13	12.0	14.6	5.2	31.8	6.6	2.1	59.5	0.40 ± 0.02
		D-11	10.1	31.9	5.6	47.6	6.2	6.1	40.1	0.40 ± 0.02
		D-10	14.4	45.2	16.0	75.6	7.8	3.1	13.5	0.41 ± 0.02
		D-9	22.5	16.6	5.2	44.3	4.5	4.2	47.0	0.41 ± 0.02
		D-6	35.4	12.0	33.5	80.9	6.4	0.8	11.9	0.40 ± 0.02
		D-5	8.5	14.7	7.1	30.3	5.3	0.8	63.6	0.41 ± 0.02
		D-3	23.4	41.4	16.7	81.5	8.1	1.6	8.8	0.40 ± 0.02
		D-2	15.3	40.0	28.1	83.4	8.8	1.7	6.1	0.41 ± 0.02
		D-1	8.9	13.3	5.2	27.4	1.7	0.4	70.5	0.41 ± 0.03

Table 3
Mineralogical compositions of the intercalation samples within the coal seam from Soma Basin based on XRD (+++ = dominant phase, ++ = abundant phase, + = minor phase, ± = detected in a few samples only).

Mineral	kM2			kM3	kP1
	Eynez	Işıklar	Deniş	Işıklar	Deniş
Quartz	+++	++	+++		+
Opal/CT		±			±
Clay Minerals	++	+++	++	+	++
Feldspar	+	+	±		±
Pyrite					±
Calcite	+	±	+	+++	+++
Aragonite			±	++	
Dolomite	+	±	±		±
Siderite		±	±		±

Table 4
Mineralogical composition of the altered tuff layers from Soma Basin based on XRD and SEM (+++ = dominant phase, ++ = abundant phase, + = minor phase, ± = detected in a few samples only, a: accessory).

Mineral	kM2		kP1
	Eynez	Işıklar	Deniş
Quartz	++	+	++
Opal/CT	±		+
Clay Minerals	+++	+++	+++
Feldspar	+		++
Biotite	a	a	a
Allanite			a
Titanite			a
Zircon	a	a	a
Pyrite	a	a	+
Sphalerite		a	a
Chalcopyrite		a	
Calcite	+		
Dolomite	±		+
Barite	a	a	a
Apatite	a	a	a
Crandallite	a	a	a
Ti-oxides		a	a

Table 5
Mineralogical composition of the coal samples from Soma Basin based on XRD and SEM (+++ = dominant phase, ++ = abundant phase, + = minor phase, ± = detected in a few samples only, a: accessory).

Mineral	kM2			kM3	kP1
	Eynez	Işıklar	Deniş	Işıklar	Deniş
Quartz	+++	+++	+++	+	++
Opal/CT	±		±	±	±
Clay Minerals	+++	++	++	++	+++
Feldspar	±	±	±	±	±
Biotite	a	a			a
Titanite					a
Zircon	a	a	a		
Pyrite	+	+	±	++	+
Sphalerite	a		a		a
Chalcopyrite	a		a		a
Gypsum				±	±
Barite	a	a	a	a	a
Calcite	++	+++	++	+++	++
Aragonite				+	±
Dolomite	±		±		±
Ankerite		a			
Siderite	±	±	±		±
Apatite	a	a	a	a	a
Monazite					a
Chromite		a			
Ti-oxides		a		a	a

Table 6

Summarized ranges and weighted averages of the elements (in μg/g, except otherwise cited) from Soma Basin and their comparison with worldwide coals (a: from Swaine, 1990; b: from Ketris and Yudovich, 2009).

Elements	kM2						kM3		kP1			
	Eynez		Işıklar		Deniş		Işıklar		Deniş		Most World Coals[a]	Clarke value (for low-rank coals)[b]
	range	avg.	range	avg.	range	avg.	range	avg.	range	avg.		
Al, %	0.13-3.91	1.93	0.03-5.5	1.3	0.31-6.0	3.8	0.09-8.4	3.9	0.24-9.3	6.2	-	-
Ca,%	0.26-1.78	1.02	0.40-9.2	1.1	0.69-6.4	1.9	0.36-10.1	4.4	0.92-13.4	1.5	-	-
Fe, %	0.03-1.01	0.51	0.08-2.4	0.5	0.24-1.2	0.68	0.09-1.9	1.18	0.17-2.2	1.4	-	-
K, %	<0.02-0.24	0.10	0.00-0.46	0.1	0.02-0.58	0.26	0.01-0.43	0.24	0.02-0.91	0.52	-	-
Mg, %	0.03-0.20	0.10	0.04-0.71	0.1	0.05-0.33	0.24	0.02-0.28	0.22	0.03-0.60	0.39	-	-
Na, %	<0.01-0.28	0.06	0.00-0.05	0.03	0.03-0.16	0.08	0.002-0.06	0.04	0.01-0.16	0.08	-	-
Li	1.3-39	19	0.53-89	19	2.5-96	51	1.6-339	137	1.35-232	139	1-80	10
Be	0.12-1.0	0.49	0.02-1.1	0.47	0.36-2.2	1.3	0.01-3.5	1.5	0.09-3.8	2.7	0.1-15	1.2
B	27-465	141	8.8-484	215	300-1813	578	36-578	372	213-956	503	5-400	56
P	22-271	158	15-1143	157	28-666	217	23-524	377	24-2074	443	10-3000	250
Sc	<0.01-7.2	2.9	<0.90-5.9	1.6	1.8-8.1	5.6	0.18-11	6.3	1.7-17	9.6	1-10	4.1
Ti	41-1671	643	7.4-1450	444	120-2176	1374	47-4009	1849	98-3501	2432	10-2000	720
V	12.3-228	93	5.7-206	74	33-221	157	9.7-296	155	37-369	266	2-100	22
Cr	2.1-35	21	0.57-51	15	9.8-60	41	2.1-84	44	4.7-99	68	0.5-60	15
Mn	7.4-130	52	6.9-320	56	9.9-228	64	2.0-50	32	6.4-173	57	5-300	100
Co	0.13-5.9	2.7	0.15-7.6	2.3	1.7-6.2	4.7	0.28-9.5	4.4	1.0-17	8.4	0.5-30	4.2
Ni	<2.4-20	7.3	0.63-25	9.8	13-31	23	<0.30-37	13	5.6-74	41	0.5-50	9.0
Cu	1.5-25	14	0.47-22	10	4.8-35	22	0.80-49	23	4.6-43	32	0.5-50	15
Zn	16-85	32	4.7-119	58	43-515	140	1.9-121	55	15.6-273	169	5-300	18
Ga	0.4-8.5	4.3	0.08-11	3.0	1.41-13	8.4	0.22-18	8.0	0.61-21	14	1-20	5.5
Ge	<0.10-1.3	0.54	0.03-1.2	0.5	0.28-1.2	0.85	0.03-2.5	1.1	0.66-4.2	1.8	1-50	2.0
As	8.8-66	37	6.0-242	70	1.8-15	6.5	0.55-25	18	3.2-22	7.6	0.5-80	7.6
Rb	0.23-41	9.5	0.21-63	9.0	1.7-54	27	0.33-34	14	0.70-70	40	2-50	10
Sr	15-140	54	3.4-223	40	18-250	99	13.1-271	189	13-523	108	15-500	120
Y	0.73-11	6.6	0.20-13.7	4.7	3.6-23	15	0.40-34	14	0.40-33	23	2-50	8.6
Zr	2.6-58	22	0.55-50	19	20-79	56	1.7-190	75	12.4-214	147	5-200	35
Nb	0.46-9.8	3.2	0.06-5.5	2.2	2.8-11.5	7.6	0.24-15	7.0	1.1-17	12	3-30	11

Table 6 (continued)

Mo	0.29-2.0	0.94	0.002-1.5	0.54	0.07-1.1	0.63	0.27-3.3	1.5	0.37-4.5	1.3	0.1-10	2.2
Cd	0.02-0.79	0.40	0.03-2.3	0.43	0.03-7.6	2.4	0.07-2.8	1.3	0.09-5.5	2.3	0.1-3	0.24
Sn	<0.14-1.4	0.41	<0.02-1.3	0.2	0.03-1.5	1.0	<0.01-2.3	0.9	0.01-2.6	1.7	1-10	0.79
Sb	0.14-0.94	0.28	<0.10-0.17	0.02	<0.02-0.44	0.15	0.02-0.4	0.3	<0.10-0.92	0.5	0.5-10	0.84
Cs	0.09-13.5	6.0	0.13-20	4.6	0.56-7.9	4.7	0.20-23	8.9	0.61-23	7.3	0.1-5	0.98
Ba	34-207	130	12-635	133	113-347	247	29-993	511	112-659	248	20-1000	150
La	1.1-15	8.4	0.1-16	5.2	3.2-25	16	0.41-49	21	0.85-48	32	1-40	10
Hf	0.09-1.7	0.64	0.01-1.5	0.5	0.28-2.2	1.4	0.05-5.1	2.1	0.11-5.1	3.6	0.4-5	1.2
Ta	0.05-0.68	0.23	0.003-0.51	0.2	0.14-1.0	0.6	0.03-1.3	0.6	0.02-1.6	1.0	0.1-2	0.26
W	0.07-2.0	0.59	<0.10-6.8	0.74	<0.34-2.9	1.5	0.21-2.3	1.1	<0.15-4.2	1.7	0.5-5	1.2
Pb	1.4-25.2	11	0.36-12	5.9	6.3-41	21	0.31-53	23	1.1-73	39	2-80	6.6
Bi	0.05-0.26	0.17	<0.01-0.16	0.03	<0.12-0.46	0.3	0.01-0.72	0.3	0.01-0.86	0.5	2-20	0.84
Ce	2.1-25	13	0.21-24	8.45	5.9-44	28	0.61-80	35	1.7-77	51	2-70	22
Pr	0.25-3.0	1.7	0.03-3.1	1.1	0.73-5.2	3.3	0.09-10	4.4	0.22-9.7	6.5	1-10	3.5
Nd	0.92-12	6.8	0.12-12	4.3	3.0-21	13	0.37-40	18	0.85-39	26.2	3-30	11
Sm	0.14-1.8	1.0	0.02-2.0	0.65	0.47-3.2	2.1	0.05-5.8	2.5	0.13-5.8	3.8	1-6	1.9
Eu	0.03-0.47	0.25	0.01-0.50	0.17	0.13-0.76	0.5	0.01-1.4	0.65	0.04-1.4	0.92	0.1-2	0.5
Gd	0.16-2.1	1.2	0.03-2.4	0.83	0.64-4.1	2.7	0.06-6.6	2.9	0.12-6.8	4.6	0-4	2.6
Tb	0.02-0.30	0.16	0.003-0.35	0.11	0.09-0.56	0.37	0.01-0.88	0.38	0.02-0.90	0.61	0.1-1	0.32
Dy	0.10-1.8	0.95	0.02-2.1	0.68	0.53-3.3	2.2	0.06-5.0	2.2	0.08-5.2	3.5	1-4	2.0
Ho	0.02-0.34	0.18	0.004-0.40	0.13	0.10-0.64	0.4	0.01-0.94	0.41	0.01-0.96	0.7	0.1-2	0.5
Er	0.06-0.95	0.49	0.01-1.1	0.36	0.25-1.8	1.1	0.03-2.5	1.1	0.03-2.6	1.8	1-3	0.85
Tm	0.01-0.17	0.08	0.002-0.20	0.06	0.05-0.31	0.20	0.01-0.43	0.19	0.01-0.45	0.31	0.5-3	0.31
Yb	0.06-1.1	0.52	0.01-1.2	0.39	0.27-1.9	1.2	0.03-2.7	1.2	0.04-2.7	1.9	0.3-3	1.0
Lu	0.01-0.17	0.09	0.002-0.21	0.07	0.05-0.32	0.20	0.01-0.45	0.20	0.01-0.46	0.3	0.03-1	0.19
Th	0.47-6.4	2.5	0.04-5.8	1.8	0.73-11	6.3	0.13-23	9.3	0.37-20	13	0.5-10	3.3
Tl	0.01-1.31	0.25	0.001-1.6	0.27	0.10-0.65	0.35	0.01-1.3	0.6	0.06-2.8	1.1	0.2-1	0.68
U	3.8-35	16	0.52-25	14	3.5-25	14	2.0-20.2	16	2.6-48	27	0.5-10	2.9

Table 7
Elemental affinities deduced from the calculation of Pearson's correlation coefficients.

Correlation with ash yield (0.70<r<1.0)
Al, K, Fe, Mg, Bi, Ce, Cu, Co, Cr, Cs, Dy, Er, Eu, Ga, Gd, Hf, Ho, La, Li, Lu, Nb, Nd, Ni, Pb, Pr, Rb, Sc, Sm, Sn, Ta, Tb, Th, Ti, Tm, Y, Yb, Zr
Correlation with ash yield (0.50<r<0.70)
Na, Cs, Cd, Ni, Ge, Pb, Sb, Tl, V, Zn
Correlation with Al content (0.70<r<1.0)
Fe, K, Mg, Be, Bi, Ce, Cu, Co, Cr, Dy, Er, Eu, Ga, Gd, Hf, Ho, La, Li, Lu, Nb, Nd, Ni, Pr, Pb, Rb, Sc, Sm, Sn, Ta, Tb, Th, Ti, Tm, V, Y, Yb, Zn, Zr
Correlation with Al content (0.50<r<0.7)
Na, Cd, Cs, Ge, Sb, Tl
Correlation with Fe content (0.70<r<1.0)
K, Be, Bi, Ce, Cu, Co, Cr, Dy, Er, Eu, Ga, Gd, Hf, Ho, La, Li, Nb, Nd, Pb, Pr, Sm, Sn, Ta, Tb, Th, Ti, Tm, Y, Zr
Correlation with Fe content (0.50<r<0.70)
Mg, Cs, Ge, Ni, Rb, Sb, Sc, Tl, V
Correlation with Ca content
Sr (0.43)
Correlation with K content (0.70<r<1.0)
Mg, Be, Bi, Ce, Cu, Co, Cr, Dy, Er, Eu, Ga, Gd, Hf, Ho, La, Li, Lu, Nb, Nd, Ni, Pb, Pr, Rb, Sc, Sm, Sn, Ta, Tb, Th, Ti, Tm, V, Y, Yb, Zn, Zr
Correlation with K content (0.50<r<0.70)
Na, Cs, Ge, Sb, Tl
Correlation with Mg content (0.70<r<1.0)
Be, Bi, Ce, Dy, Er, Eu, Ga, Gd, Hf, Ho, La, Lu, Nb, Nd, Pb, Pr, Rb, Sm, Sn, Ta, Tb, Th, Ti, Tm, Y, Yb, Zr
Correlation with Mg content (0.50<r<0.70)
Cr, Co, Cu, Li, Ni, Sc, V, Zn
Correlation with Na content (0.50<r<1.0)
Be, Bi, Ce, Dy, Er, Eu, Ga, Gd, Ho, La, Nb, Nd, Pb, Pr, Rb, Sm, Sn, Ta, Th, Tm, Y, Tb, Zn

Fig. 1. a) Geological map of surrounding area of the Soma Basin (modified from İnci, 1998a, Karayiğit, 1998); b) Stratigraphic column of the Soma Basin (modified and simplified from Karayiğit and Whatley, 1997, İnci, 1998a).

Fig. 2. Stratigraphic column of the studied profiles in the Soma Basin.

Fig. 3. Photomicrographs of Soma coal. Textinite (T), texto-ulminite (TU), ulminite (U), densinite (D), attrinite (A), corpohuminite (CH), gelinite (Gel), levigelinite (LG), porigelinite, fusinite (Fus), inertodetrinite (Id) resinite (R), sporinite (Sp), suberinite (Sub), and siderite (Sd). All photomicrographs are taken under incident white light (a, c, e, f, g, h), oil immersion, 500x total magnification.

Fig. 4. a) Pseudo-Van Krevelen diagram, b) plot of HI against T_{max} of the coal samples (after Peters, 1986)

Fig. 5. The Soma coals plotted in the HI-VR diagram (after Petersen, 2006).

Fig. 6. Gas chromatograms of the aromatic hydrocarbon fractions of a) sample E-9 from kM2 seam and b) sample D-6 from kP1 seam (*n*-alkanes are indicated by their carbon chain length, pri: pristine, phy: pjytane).

Fig. 7. SEM backscattered images of crystalline phases in the altered volcanic ash samples. a) K-feldspar (2), zircon (1 and 5) and apatite (4) associated with kaolinite (3); b) plagioclase (1) and apatite associated with kaolinite (5), kaolinite (2) within biotite (2); c) plagioclase (Pl) and secondary dolomite (Dol) around kaolinite (Kln); d) apatite (Ap), alkali feldspar (Afs) and plagioclase (Pl) associated with kaolinite (Kln); e) apatite (Ap) within plagioclase (Pl), and individual kaolinite (Kln); f) pyrite (Py) blades and apatite (Ap) within kaolinite (Kln).

Fig. 8. SEM backscattered images of crystalline phases in the altered volcanic ash samples. a) individual (vermicules?) kaolinite (Kln) and biotite (Bt); b) non-altered biotite (Bt), K-feldspar (Kfs) and pyrite (Py); c) quartz (Qtz), K-feldspar (Kfs) and titanite (Ttn) associated with kaolinite (Kln); d) kaolinite (Kln) around possibly altered biotite (Bt) and plagioclase (Pl).

Fig. 9. SEM backscattered images of crystalline phases in the coal samples. a, b and c) apatite (Ap), siderite (Sd), zircon (Zrn) plagioclase (Pl) K-feldspar (Kfs) and alkali feldspar (Afs) associated with kaolinite (Kln); d) ilmenite crystals within cavities of K-feldspar; e) quartz (Qtz), Ca-REE phosphate (crandallite?) and kaolinite (Kln) within organic matter (detrohuminite?); f) fossil bone-fragment (Ca-phosphate composition).

Fig. 10. SEM backscattered images of crystalline phases in the coal samples. a) K-feldspar (Kln) and kaolinite associated with syngenetic calcite (Cal); b) microprobe element mapping of image a; c) calcite (Cal) and replacement carbonates; d) 1: calcite, 2: dolomite and siderite association, 3: calcite and siderite association; e) epigenetic dolomite (Dol); f) calcareous fossil shell remains and apatite (Ap).

Fig. 11. SEM backscattered images, and selected EDX data and microprobe element mapping of crystalline phases in the coal samples images. a) siderites (Sd) within the cavities of organic matter (telohuminite?); b) siderites (Sd) around dolomites (Dol), and individual silica, K-feldspar (Kfs) and alkali feldspar (Afs) crystals; c) microprobe element mapping of pyrite (Py) and siderite (Sd); e) EDX data for siderite in the image d; e) dolomite (Dol) around siderite (Sd); f) EDX data for dolomite in the image e.

Fig. 12. SEM backscattered images of crystalline phases in the coal samples. a) epigenetic sphalerite (Sp) within kaolinite (Kln); b) As-bearing pyrites (py) within kaolinite; c) epigenetic chalcopyrites (Ccp) within feldspar (Fsp); epigenetic pyrite (Py) within alkali feldspar (Afs); e) pyrites (Py) within the cavities of calcareous fossil shell remain; f) epigenetic barite.

Fig. 13. Plot of HI vs. T_{max} of Soma coal (after Sykes and Snowdon, 2002).

Fig. 14. ABC ternary plot of the coal samples from sampling profile (after Mukhopadhyay, 1989).

Fig. 15. GI vs. TPI plot of the coal samples from sampling profile (after Diessel, 1992, as modified by Kalaitzidis et al., 2004).

Fig. 15. VI vs. GWI plot of the coal samples from sampling profile (after Calder et al., 1991, as modified by Kalaitzidis et al., 2004).

Figure 1

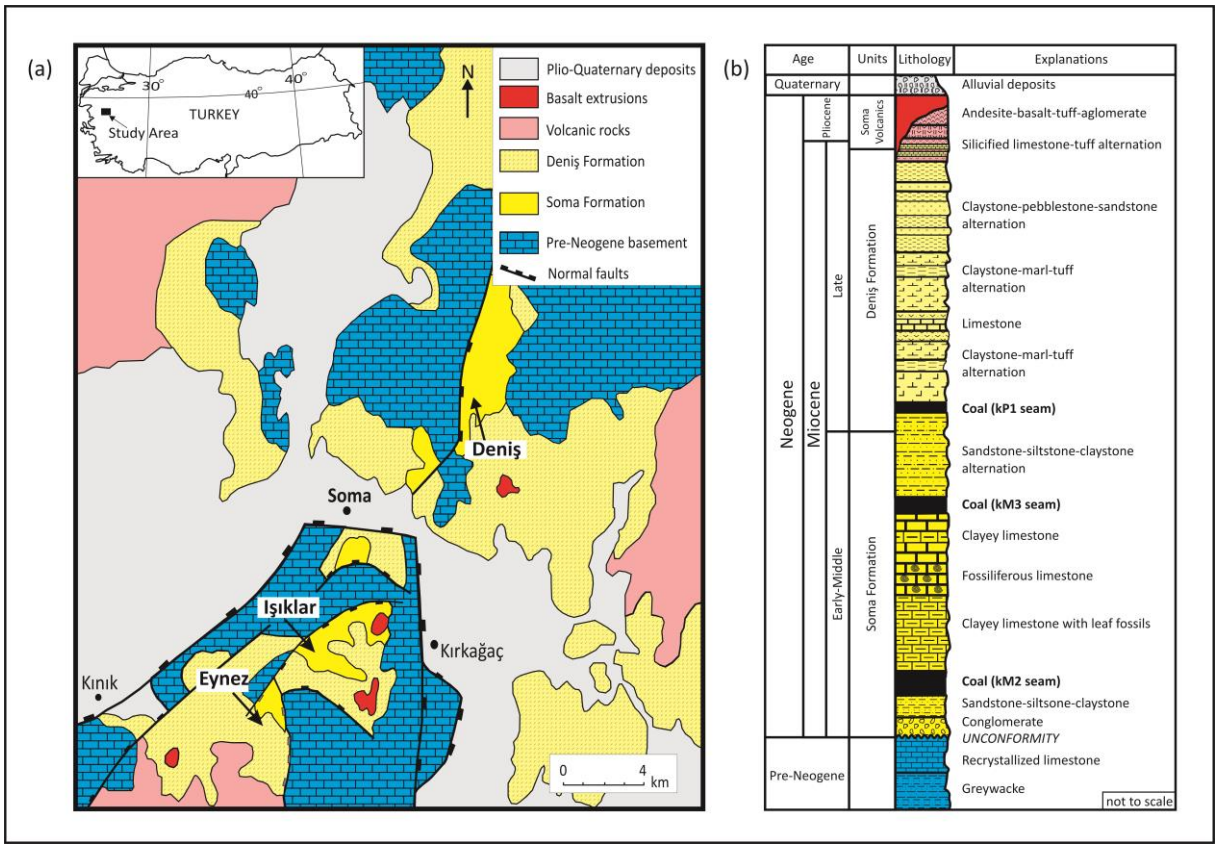
(a)
30°
40°
40°
TURKEY
Study Area
N
Plio-Quaternary deposits
Basalt extrusions
Volcanic rocks
Deniş Formation
Soma Formation
Pre-Neogene basement
Normal faults
Deniş
Soma
Işıklar
Kırkağaç
Kınık
Eynez
0
4
km
(b)
Age
Units
Lithology
Explanations
Quaternary
Alluvial deposits
Neogene
Miocene
Pliocene
Late
Early-Middle
Soma Volcanics
Deniş Formation
Soma Formation
Andesite-basalt-tuff-aglomerate
Silicified limestone-tuff alternation
Claystone-pebblestone-sandstone alternation
Claystone-marl-tuff alternation
Limestone
Claystone-marl-tuff alternation
Coal (kP1 seam)
Sandstone-siltstone-claystone alternation
Coal (kM3 seam)
Clayey limestone
Fossiliferous limestone
Clayey limestone with leaf fossils
Coal (kM2 seam)
Sandstone-siltsone-claystone
Conglomerate
UNCONFORMITY
Pre-Neogene
Recrystallized limestone
Greywacke
not to scale

Figure 2

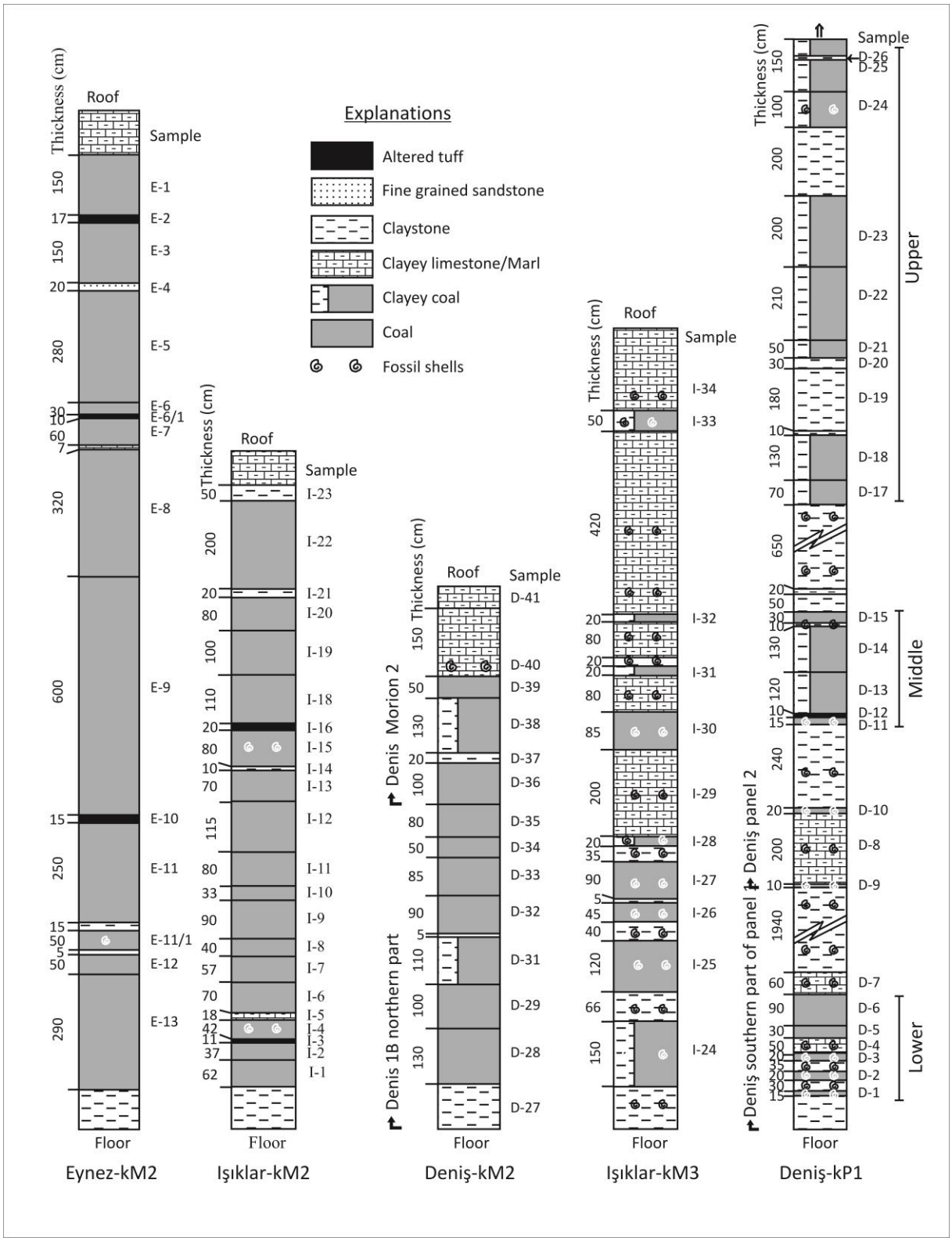
Explanations
Altered tuff
Fine grained sandstone
Claystone
Clayey limestone/Marl
Clayey coal
Coal
Fossil shells
Thickness (cm)
Roof
Sample
Floor
Eynez-kM2
Işıklar-kM2
Denis 1B northern part
Denis Morion 2
Deniş-kM2
Işıklar-kM3
Deniş southern part of panel 1
Deniş panel 2
Deniş-kP1
Upper
Middle
Lower

Figure 3

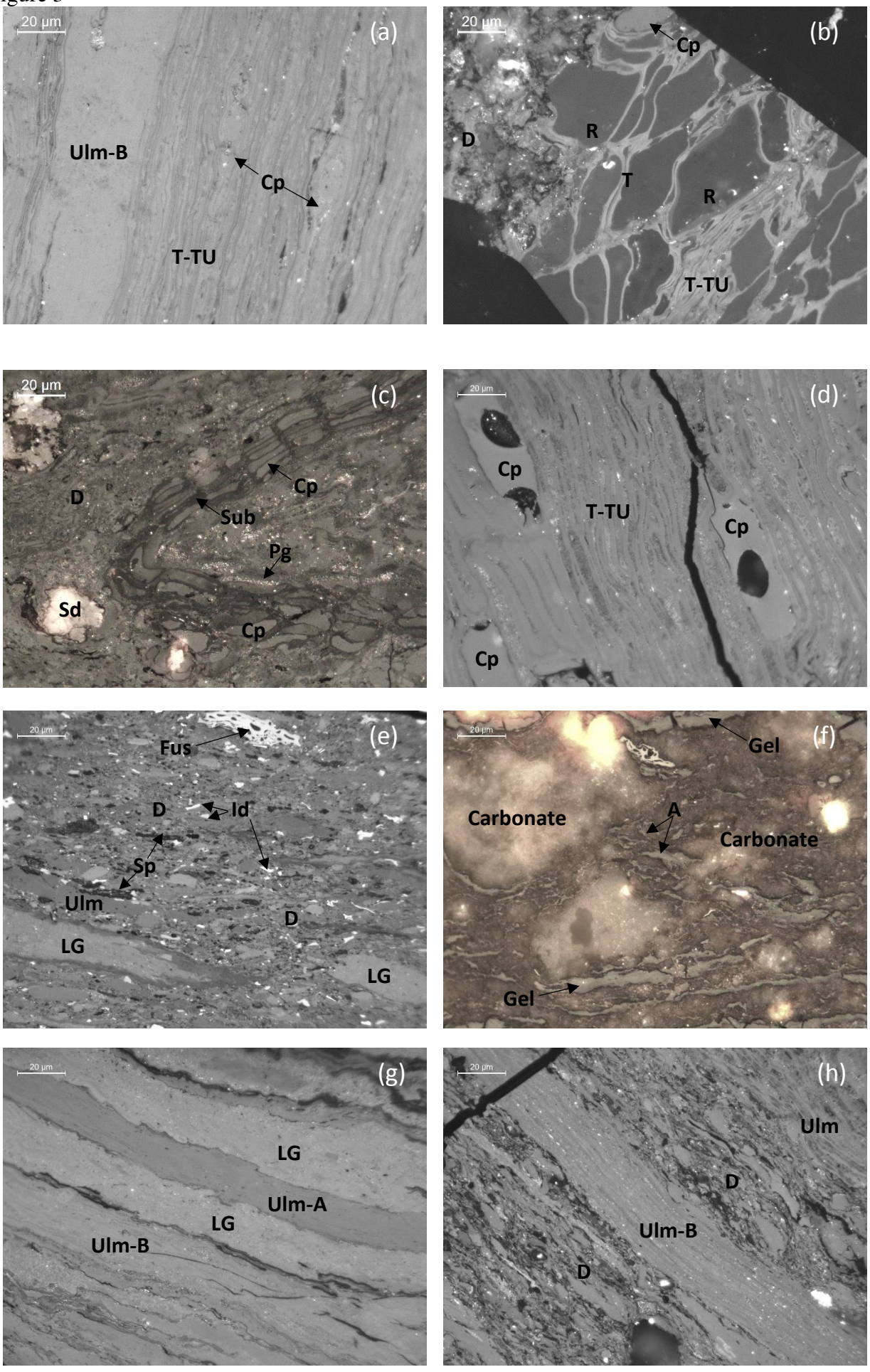
20 µm
(a)
Ulm-B
Cp
T-TU
20 µm
(b)
Cp
D
R
T
R
T-TU
20 µm
(c)
D
Cp
Sub
Pg
Sd
Cp
20 µm
(d)
Cp
T-TU
Cp
Cp
20 µm
(e)
Fus
D
Id
Sp
Ulm
D
LG
LG
20 µm
(f)
Gel
Carbonate
A
Carbonate
Gel
20 µm
(g)
LG
Ulm-A
LG
Ulm-B
20 µm
(h)
Ulm
D
Ulm-B
D

Figure 4

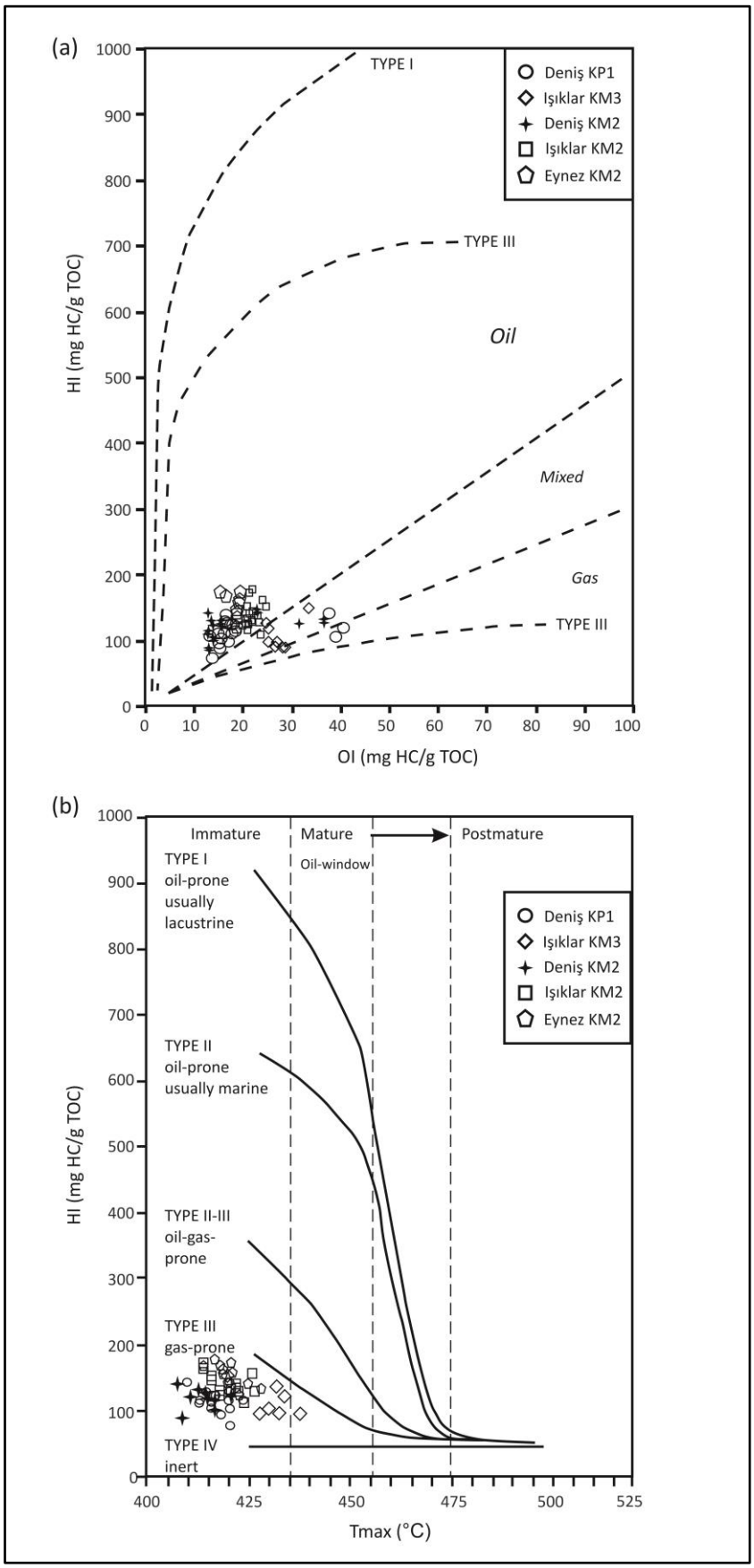
(a)
TYPE I
TYPE III
Oil
Mixed
Gas
TYPE III
Deniş KP1
Işıklar KM3
Deniş KM2
Işıklar KM2
Eynez KM2
HI (mg HC/g TOC)
OI (mg HC/g TOC)
(b)
Immature
Mature
Oil-window
Postmature
TYPE I
oil-prone
usually
lacustrine
TYPE II
oil-prone
usually marine
TYPE II-III
oil-gas-
prone
TYPE III
gas-prone
TYPE IV
inert
Tmax (°C)

Figure 5

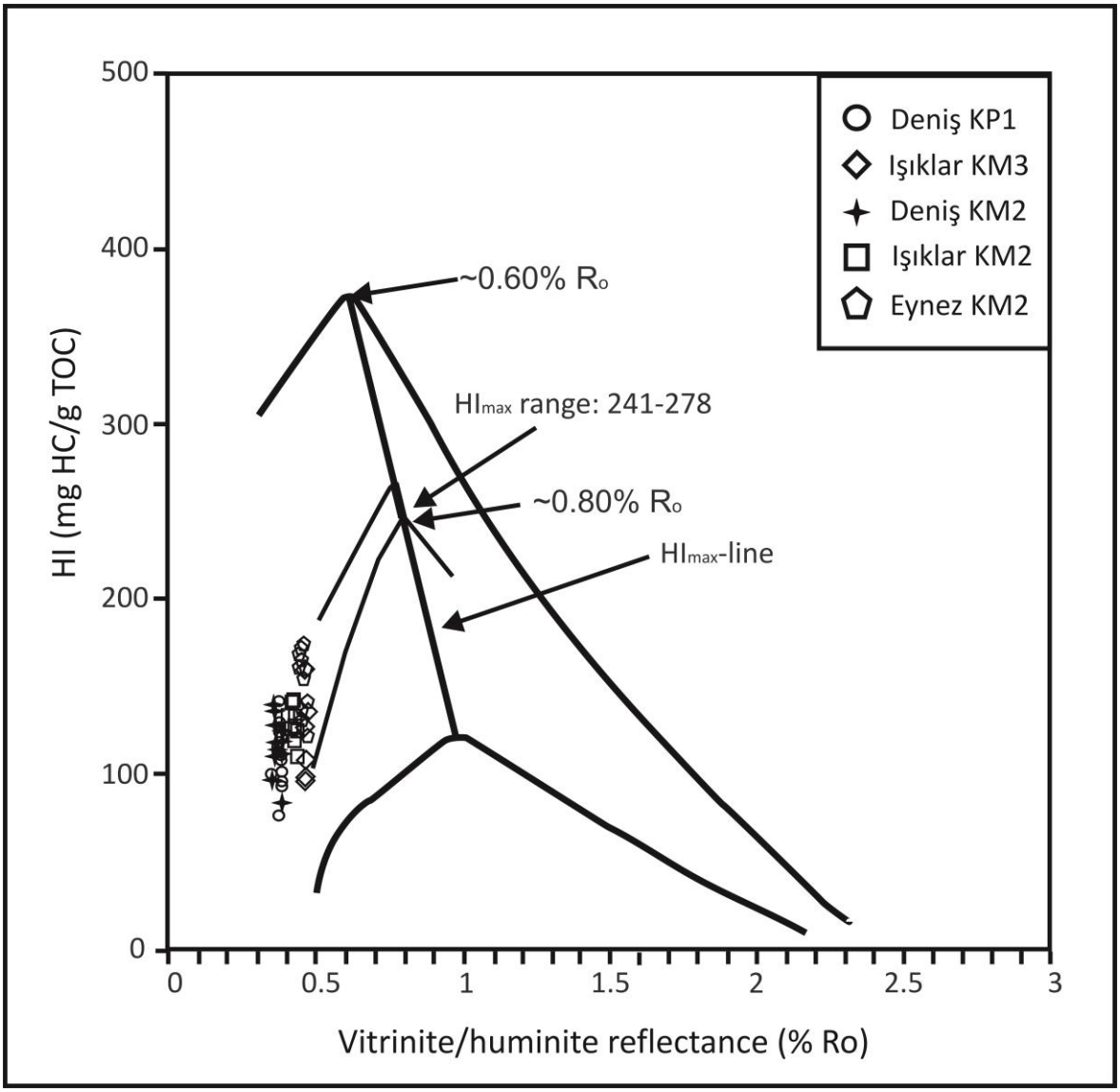
Deniş KP1
Işıklar KM3
Deniş KM2
Işıklar KM2
Eynez KM2
~0.60% Ro
HImax range: 241-278
~0.80% Ro
HImax-line
HI (mg HC/g TOC)
Vitrinite/huminite reflectance (% Ro)
0
100
200
300
400
500
0
0.5
1
1.5
2
2.5
3

Figure 6

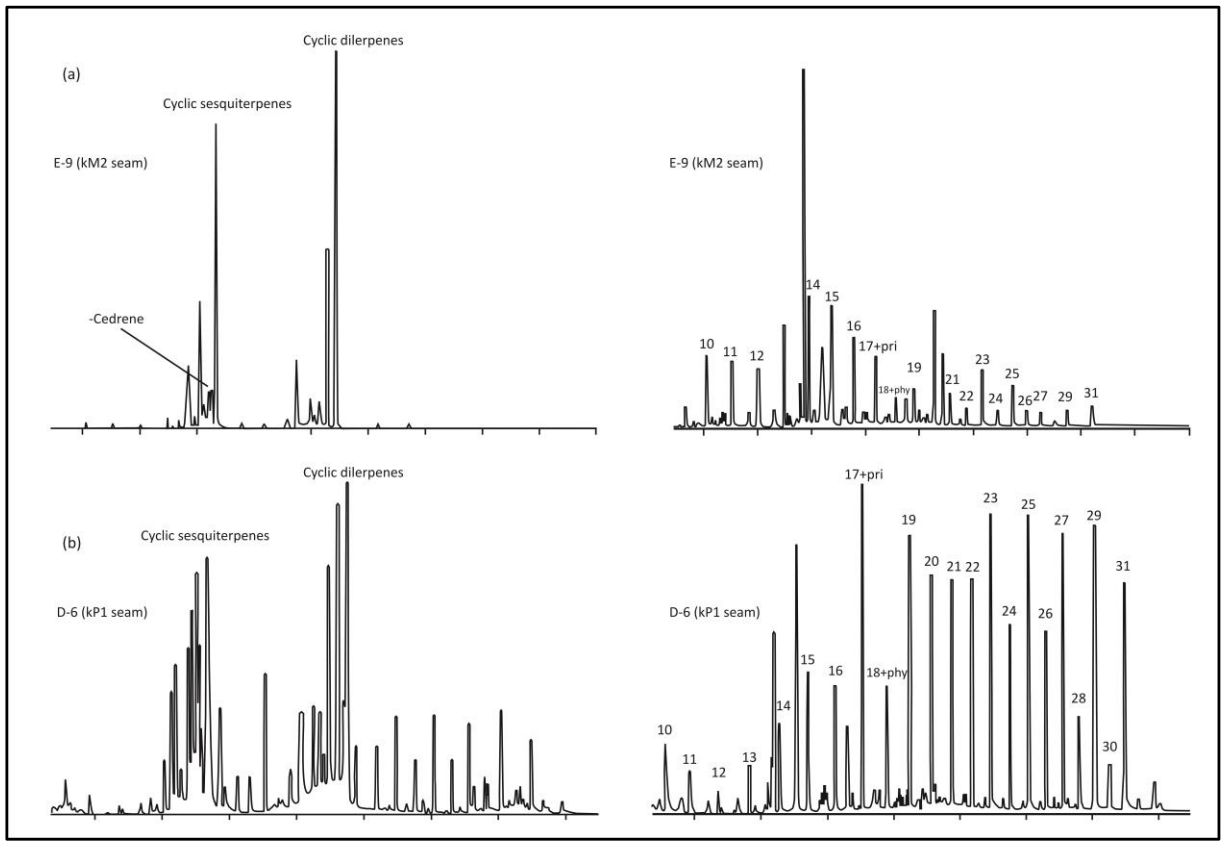
(a)
Cyclic dilerpenes
Cyclic sesquiterpenes
E-9 (kM2 seam)
-Cedrene
E-9 (kM2 seam)
10
11
12
14
15
16
17+pri
18+phy
19
21
22
23
24
25
26
27
29
31
(b)
Cyclic dilerpenes
Cyclic sesquiterpenes
D-6 (kP1 seam)
D-6 (kP1 seam)
10
11
12
13
14
15
16
17+pri
18+phy
19
20
21
22
23
24
25
26
27
28
29
30
31

Figure 7

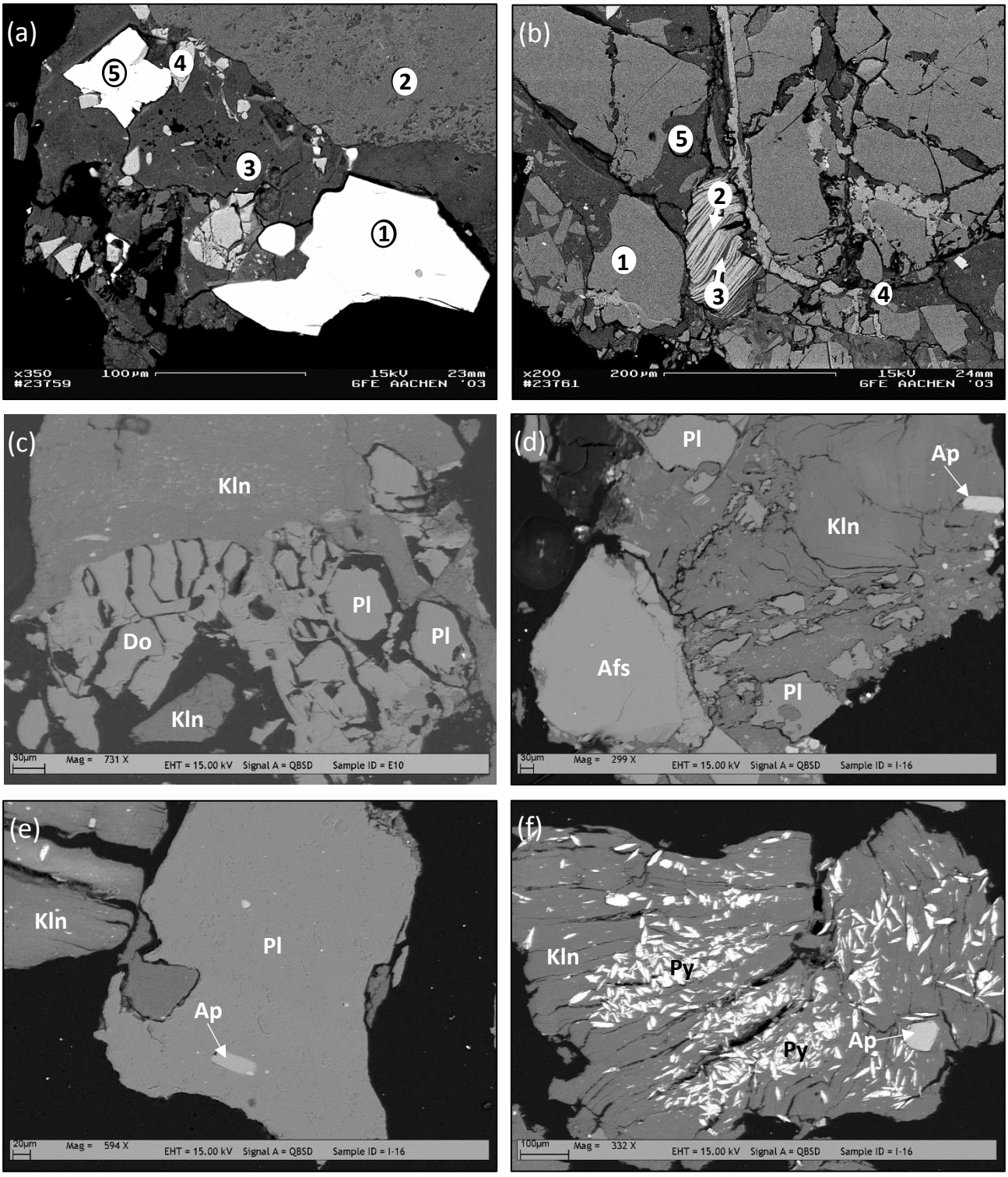
(a)
5
4
2
3
1
×350 100µm 15kV 23mm
#23759 GFE AACHEN '03
(b)
5
5
2
1
3
4
×200 200µm 15kV 24mm
#23761 GFE AACHEN '03
(c)
Kln
Pl
Do
Pl
Kln
30µm Mag = 731 X EHT = 15.00 kV Signal A = QBSD Sample ID = E10
(d)
Pl
Ap
Kln
Afs
Pl
30µm Mag = 299 X EHT = 15.00 kV Signal A = QBSD Sample ID = I-16
(e)
Kln
Pl
Ap
20µm Mag = 594 X EHT = 15.00 kV Signal A = QBSD Sample ID = I-16
(f)
Kln
Py
Py
Ap
100µm Mag = 332 X EHT = 15.00 kV Signal A = QBSD Sample ID = I-16

Figure 8

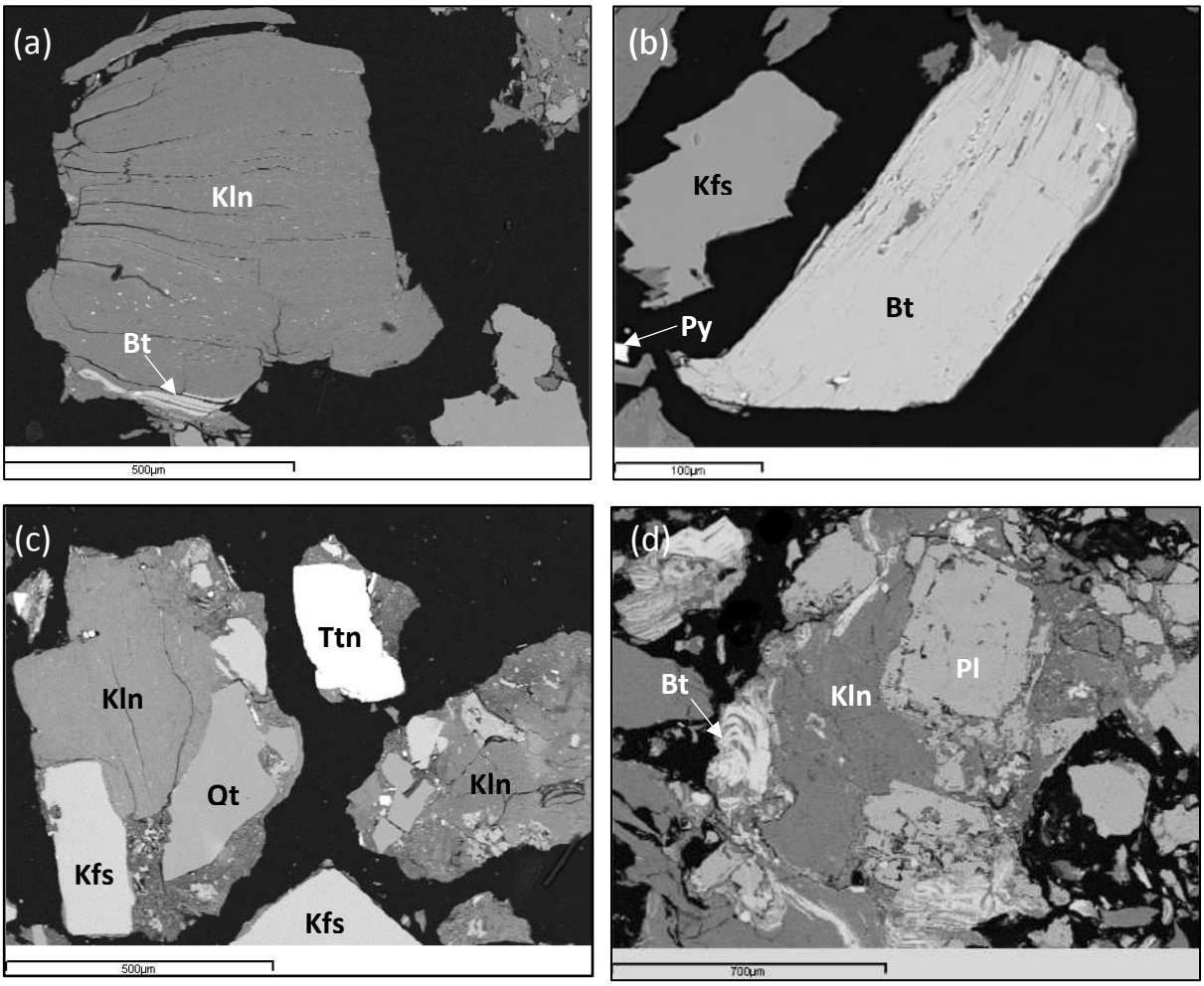
(a)
Kln
Bt
500µm
(b)
Kfs
Bt
Py
100µm
(c)
Ttn
Kln
Qt
Kln
Kfs
Kfs
500µm
(d)
Bt
Kln
Pl
700µm

Figure 9

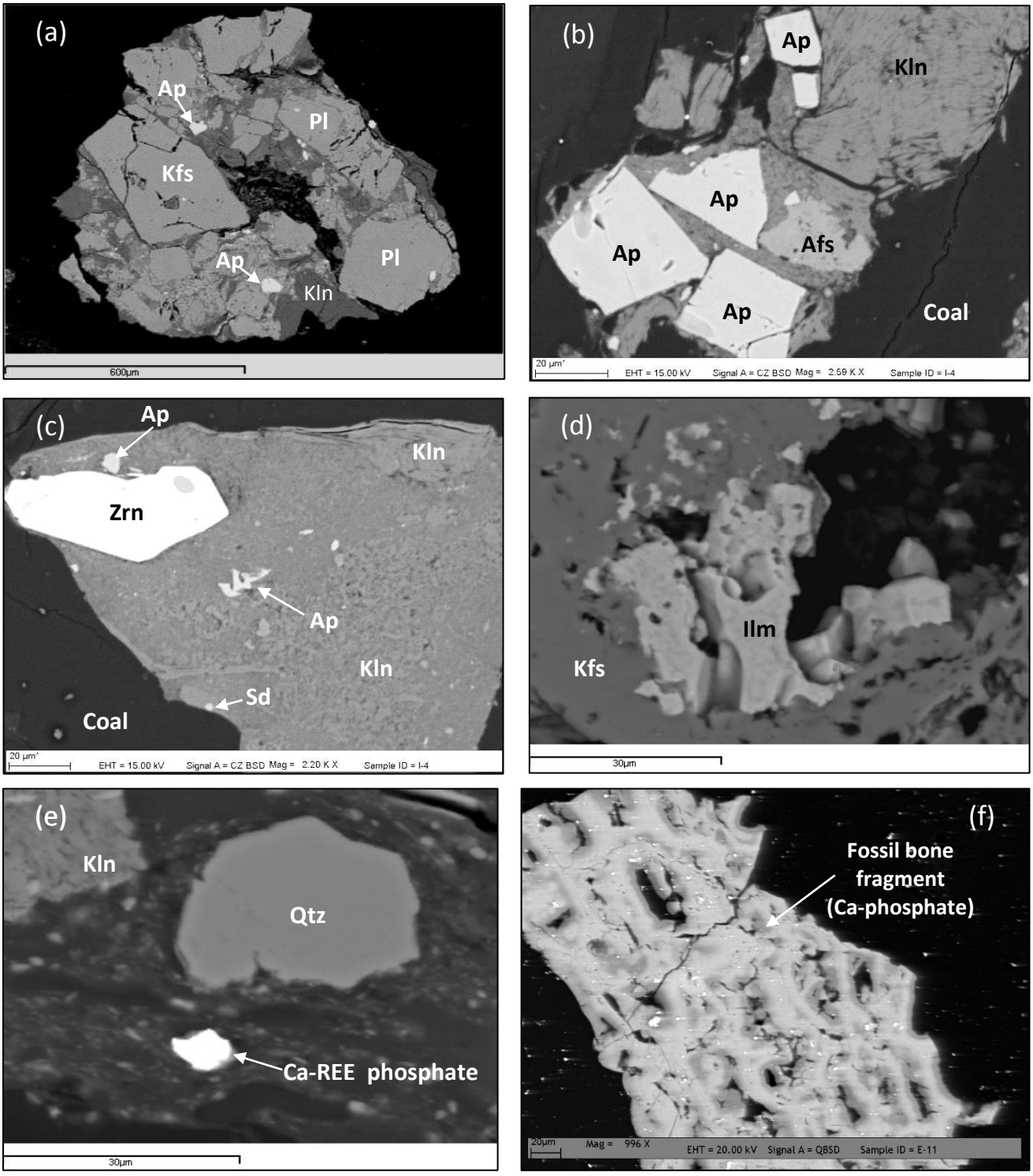
(a)
Ap
Pl
Kfs
Ap
Pl
Kln
600µm
(b)
Ap
Kln
Ap
Ap
Afs
Ap
Coal
20 µm
EHT = 15.00 kV
Signal A = CZ BSD
Mag = 2.69 K X
Sample ID = I-4
(c)
Ap
Kln
Zrn
Ap
Kln
Sd
Coal
20 µm
EHT = 15.00 kV
Signal A = CZ BSD
Mag = 2.20 K X
Sample ID = I-4
(d)
Ilm
Kfs
30µm
(e)
Kln
Qtz
Ca-REE phosphate
30µm
(f)
Fossil bone
fragment
(Ca-phosphate)
20µm
Mag = 996 X
EHT = 20.00 kV
Signal A = QBSD
Sample ID = E-11

Figure 10

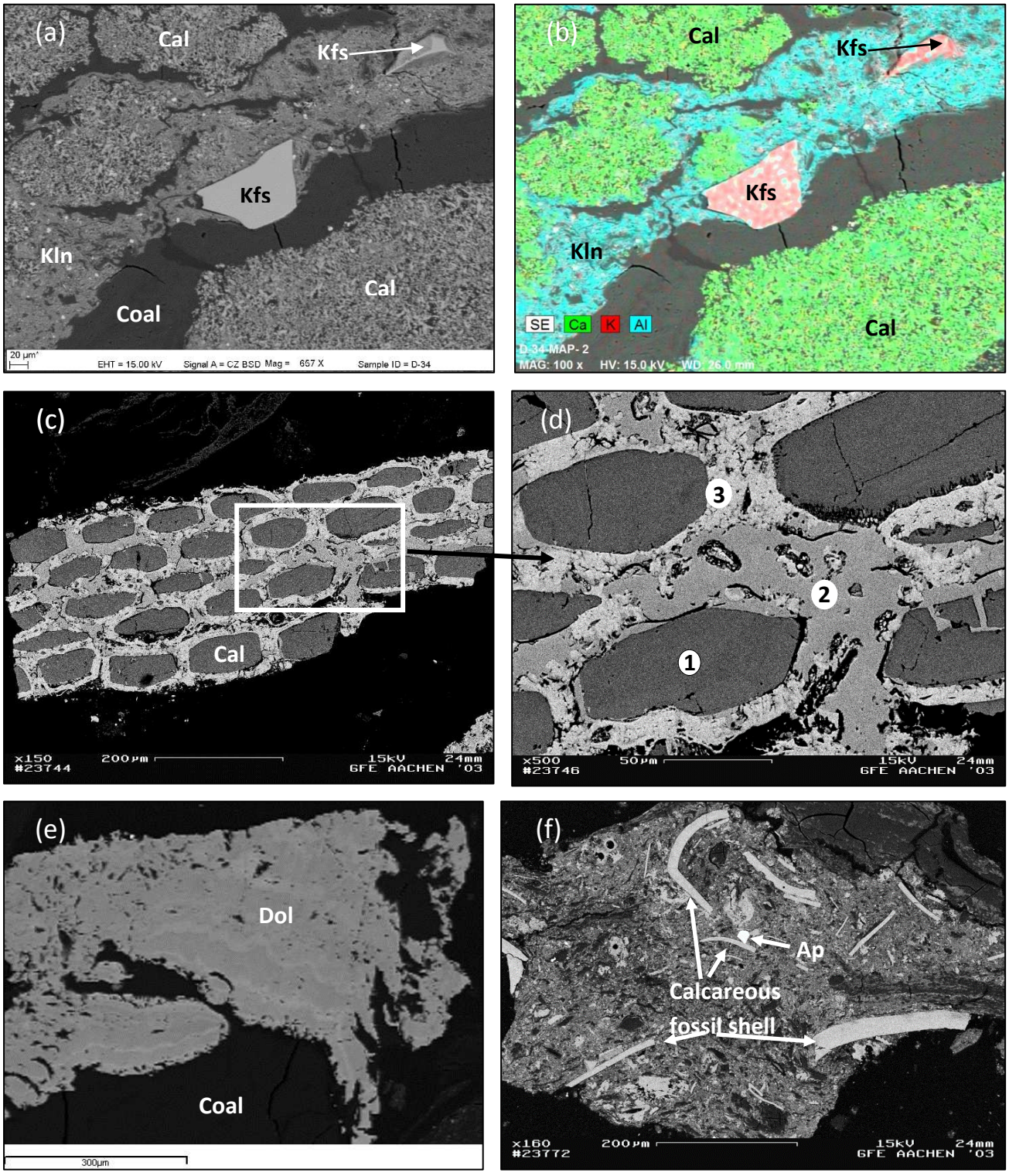
(a)
Cal
Kfs
Kfs
Kln
Cal
Coal
20 µm
EHT = 15.00 kV
Signal A = CZ BSD Mag = 657 X
Sample ID = D-34
(b)
Cal
Kfs
Kfs
Kln
SE
Ca
K
Al
Cal
D-34-MAP- 2
MAG: 100 x
HV: 15.0 kV
WD: 26.0 mm
(c)
Cal
x150
#23744
200 µm
15kV
24mm
GFE AACHEN '03
(d)
3
2
1
x500
#23746
50 µm
15kV
24mm
GFE AACHEN '03
(e)
Dol
Coal
300µm
(f)
Ap
Calcareous
fossil shell
x160
#23772
200 µm
15kV
24mm
GFE AACHEN '03

Figure 11

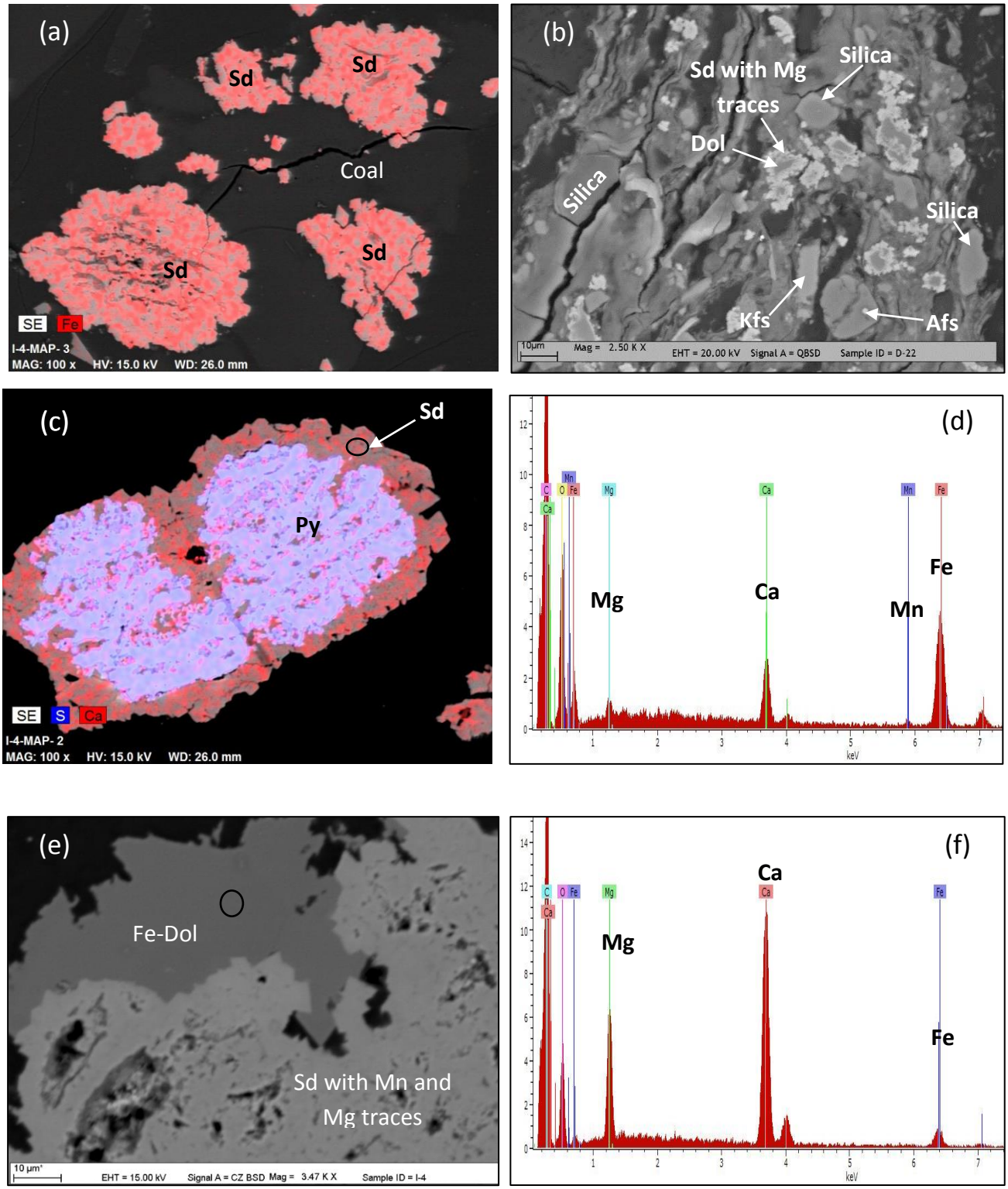
(a)
Sd
Sd
Coal
Sd
Sd
SE Fe
I-4-MAP- 3
MAG: 100 x HV: 15.0 kV WD: 26.0 mm
(b)
Sd with Mg traces
Silica
Dol
Silica
Silica
Kfs
Afs
10µm Mag = 2.50 K X EHT = 20.00 kV Signal A = QBSD Sample ID = D-22
(c)
Sd
Py
SE S Ca
I-4-MAP- 2
MAG: 100 x HV: 15.0 kV WD: 26.0 mm
(d)
Mg
Ca
Mn
Fe
keV
(e)
Fe-Dol
Sd with Mn and Mg traces
10 µm EHT = 15.00 kV Signal A = CZ BSD Mag = 3.47 K X Sample ID = I-4
(f)
Ca
Mg
Fe
keV

Figure 12

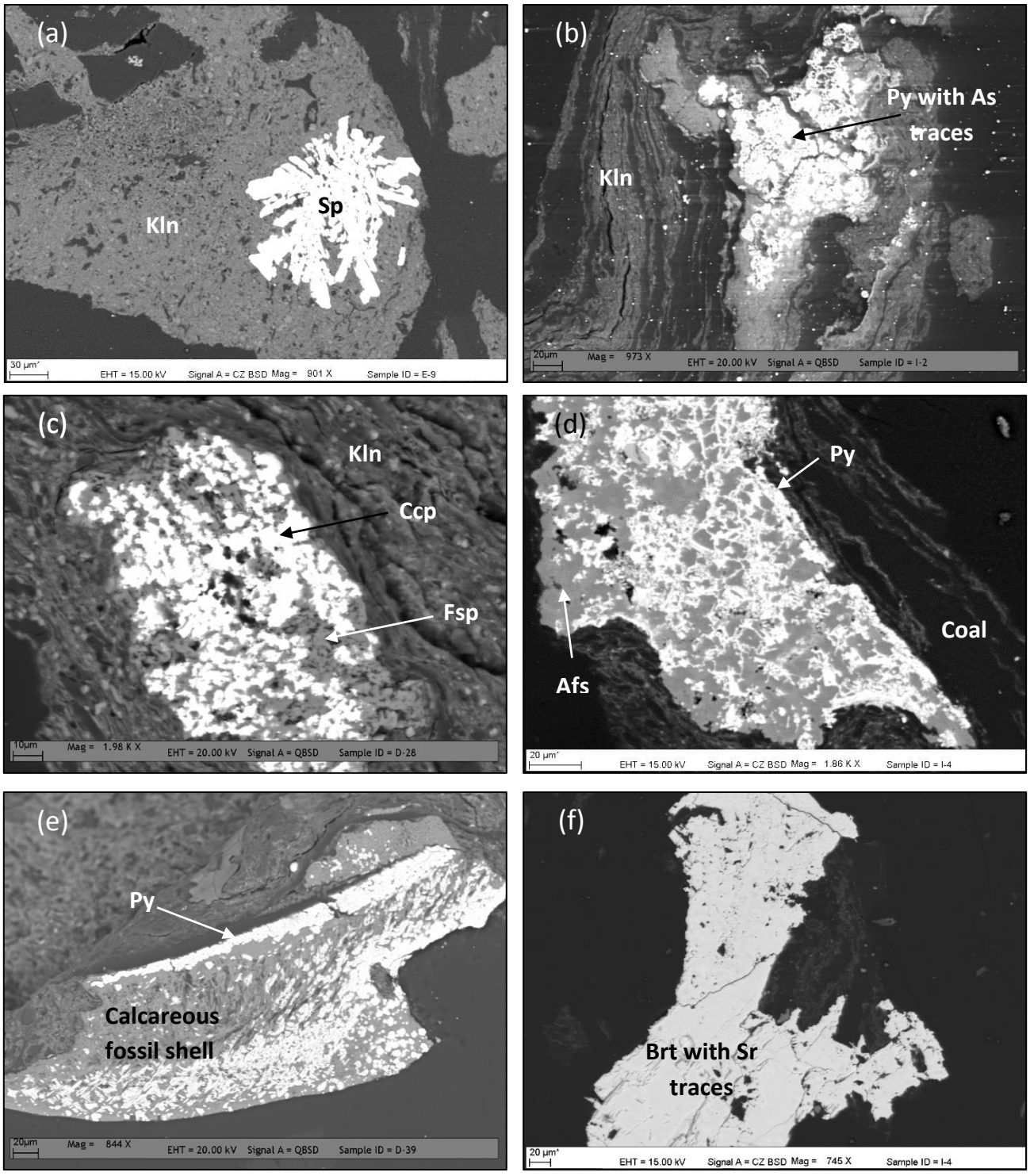
(a)
Kln
Sp
30 µm
EHT = 15.00 kV Signal A = CZ BSD Mag = 901 X Sample ID = E-9
(b)
Py with As traces
Kln
20µm
Mag = 973 X EHT = 20.00 kV Signal A = QBSD Sample ID = I-2
(c)
Kln
Ccp
Fsp
10µm
Mag = 1.98 K X EHT = 20.00 kV Signal A = QBSD Sample ID = D-28
(d)
Py
Coal
Afs
20 µm
EHT = 15.00 kV Signal A = CZ BSD Mag = 1.86 K X Sample ID = I-4
(e)
Py
Calcareous fossil shell
20µm
Mag = 844 X EHT = 20.00 kV Signal A = QBSD Sample ID = D-39
(f)
Brt with Sr traces
20 µm
EHT = 15.00 kV Signal A = CZ BSD Mag = 745 X Sample ID = I-4

Figure 13

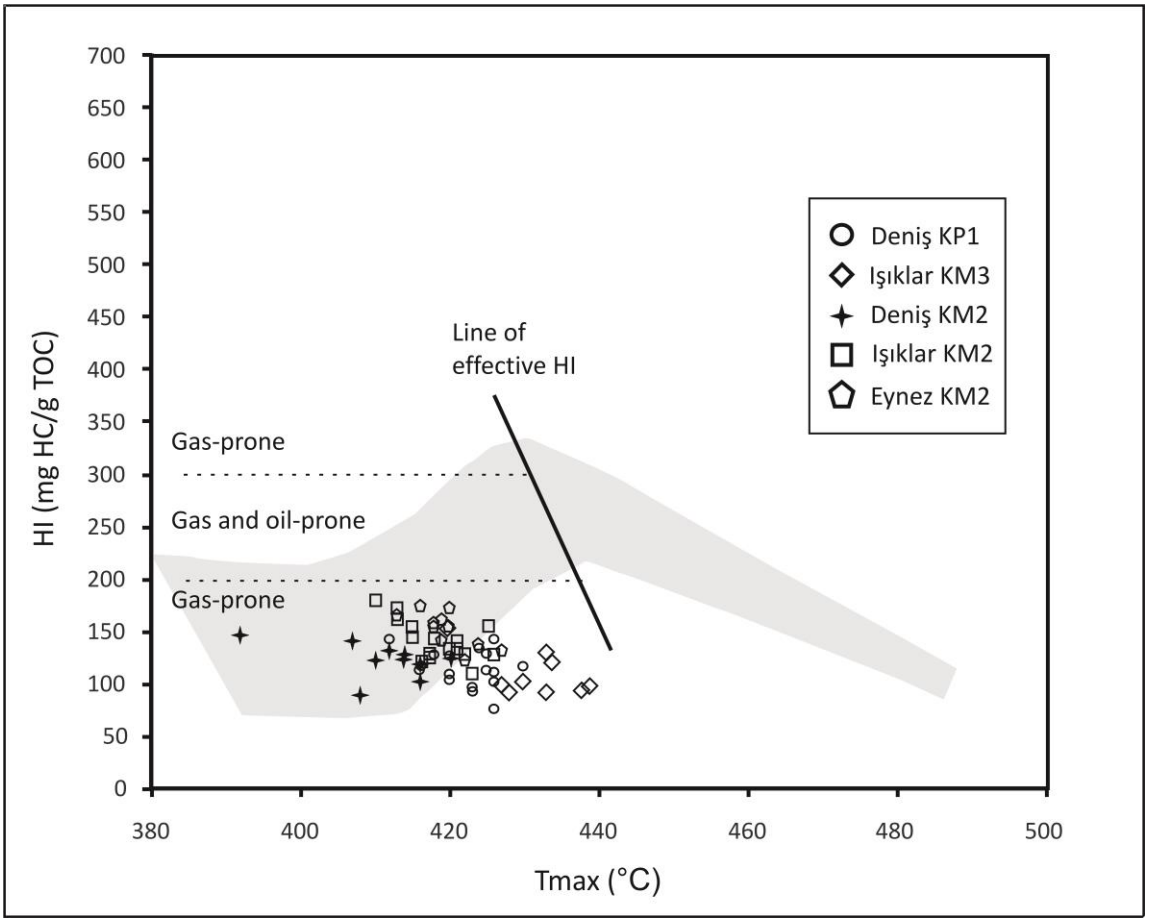
HI (mg HC/g TOC)
Tmax (°C)
700
650
600
550
500
450
400
350
300
250
200
150
100
50
0
380
400
420
440
460
480
500
Line of
effective HI
Gas-prone
Gas and oil-prone
Gas-prone
Deniş KP1
Işıklar KM3
Deniş KM2
Işıklar KM2
Eynez KM2

Figure 14

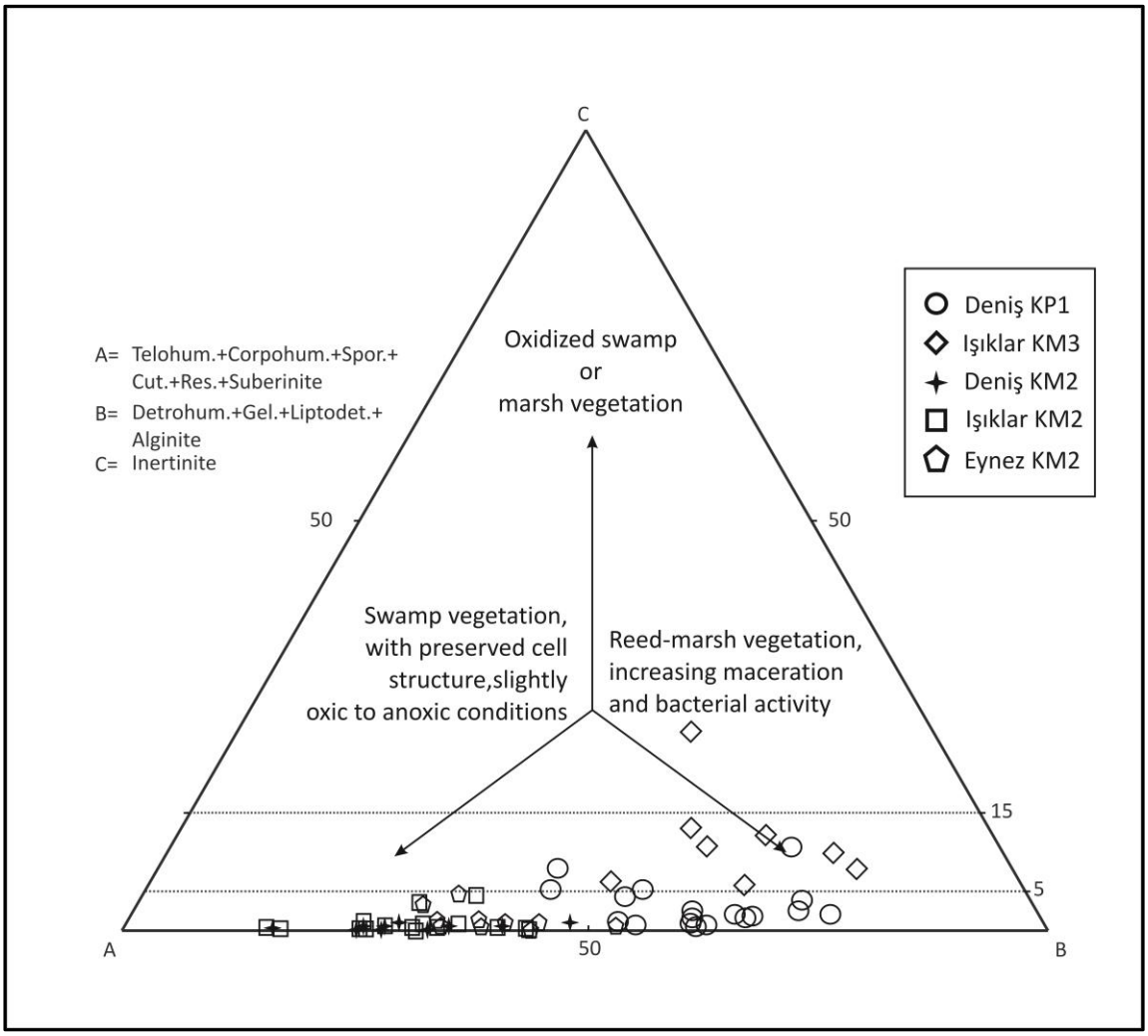
C
A= Telohum.+Corpohum.+Spor.+
Cut.+Res.+Suberinite
B= Detrohum.+Gel.+Liptodet.+
Alginite
C= Inertinite
Oxidized swamp
or
marsh vegetation
Deniş KP1
Işıklar KM3
Deniş KM2
Işıklar KM2
Eynez KM2
50
50
Swamp vegetation,
with preserved cell
structure,slightly
oxic to anoxic conditions
Reed-marsh vegetation,
increasing maceration
and bacterial activity
15
5
A
50
B

Figure 15

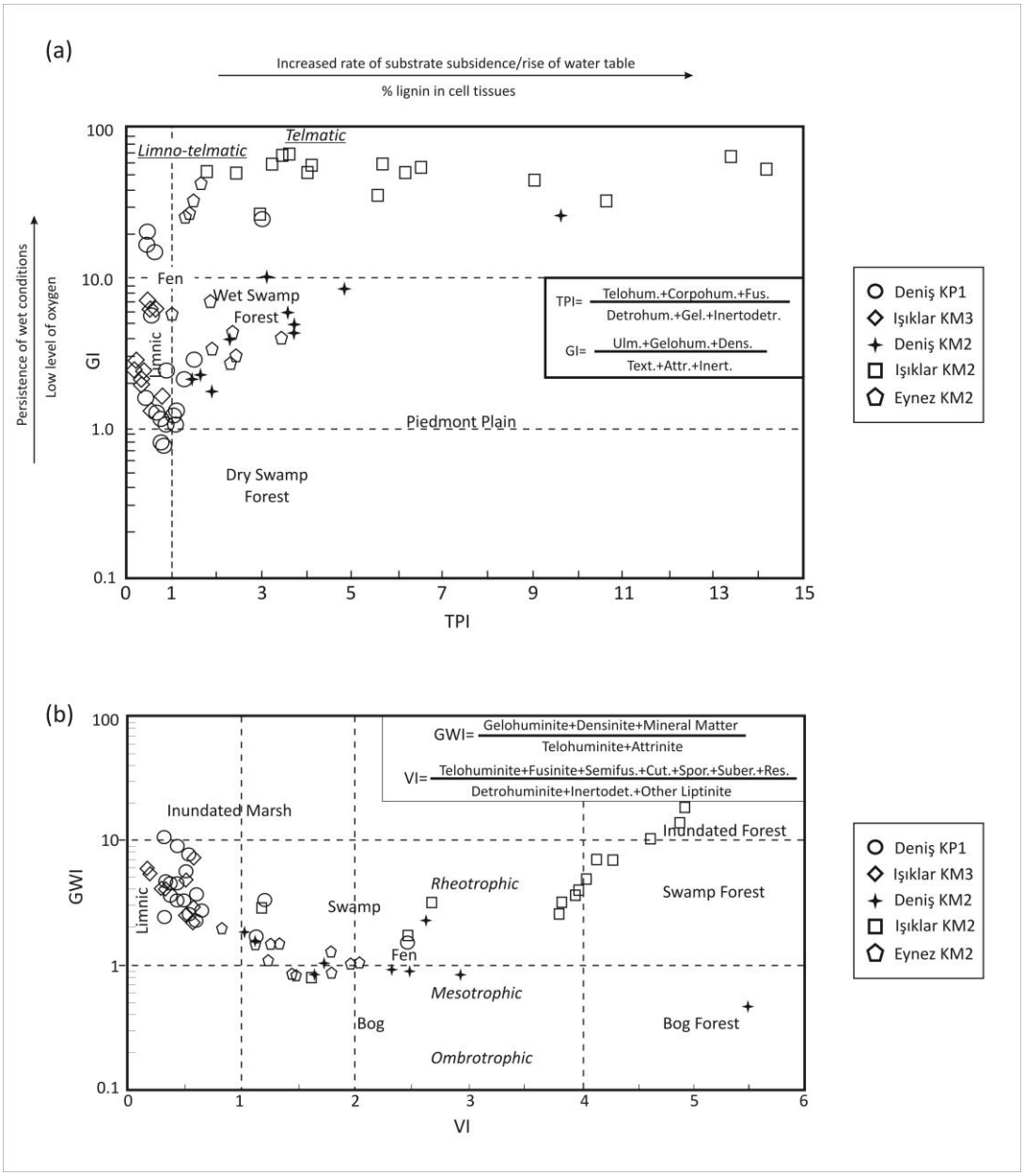
(a)
Increased rate of substrate subsidence/rise of water table
% lignin in cell tissues
Persistence of wet conditions
Low level of oxygen
GI
TPI
Limno-telmatic
Telmatic
Fen
Wet Swamp Forest
Limnic
Piedmont Plain
Dry Swamp Forest
TPI= Telohum.+Corpohum.+Fus. / Detrohum.+Gel.+Inertodetr.
GI= Ulm.+Gelohum.+Dens. / Text.+Attr.+Inert.
Deniş KP1
Işıklar KM3
Deniş KM2
Işıklar KM2
Eynez KM2
(b)
GWI
VI
GWI= Gelohuminite+Densinite+Mineral Matter / Telohuminite+Attrinite
VI= Telohuminite+Fusinite+Semifus.+Cut.+Spor.+Suber.+Res. / Detrohuminite+Inertodet.+Other Liptinite
Inundated Marsh
Inundated Forest
Swamp Forest
Rheotrophic
Swamp
Fen
Limnic
Mesotrophic
Bog
Bog Forest
Ombrotrophic
Deniş KP1
Işıklar KM3
Deniş KM2
Işıklar KM2
Eynez KM2